Quaternary Science Reviews 201 (2018) 57–76

Contents lists available at ScienceDirect

Quaternary Science Reviews

journal homepage: www.elsevier.com/locate/quascirev

Millennial-scale East Asian monsoon variability of the last glacial deduced from annually laminated sediments from Lake Sihailongwan, N.E. China

Jens Mingram [a, *], Martina Stebich [b], Georg Schettler [a], Yaqin Hu [a, e], Patrick Rioual [d], Norbert Nowaczyk [a], Peter Dulski [a, f], Haitao You [c], Stephan Opitz [g], Qiang Liu [d], Jiaqi Liu [d]

[a] GFZ German Research Centre for Geosciences, Telegrafenberg C323, 14473, Potsdam, Germany
[b] Senckenberg Research Institute and Natural History Museum Frankfurt – Research Station of Quarternary Palaeontology, Weimar, Germany
[c] Graduate School of the Chinese Academy of Sciences, Beijing, China
[d] Institute of Geology and Geophysics, Chinese Academy of Sciences, Beijing, China
[e] BotanyLabyahu, Grünheide/Mark, Germany
[f] Seegefelder Weg 335c, Berlin, Germany
[g] Institute of Geography, University of Cologne, Cologne, Germany

ARTICLE INFO

Article history:
Received 31 January 2018
Received in revised form
23 August 2018
Accepted 16 September 2018
Available online 19 October 2018

Keywords:
Paleoclimatology
East Asian monsoon
Lake sediments
Varves
Pleistocene
Dansgaard-Oeschger cycles
Heinrich events

ABSTRACT

Lake Sihailongwan in Jilin province, NE China, provides the first continuous and almost entirely seasonally laminated sediment record on the East Asian mainland comprising the complete Holocene, the Late-glacial period, and large parts of the Last Glacial. Sediment and palynological proxy data provide a finely resolved regional environmental history of the East Asian monsoon. A varve-based chronology (shl-vc2) has been established for the last 65,000 years and allows a detailed comparison with other long regional and global palaeoclimate records. Vegetation density of the study area depends, on the long run, on precessionally forced insolation changes, with superimposed millennial-scale variability during the Last Glacial. Periodic increase of organic carbon content and thermophilous tree species like *Ulmus* and *Fraxinus* and contemporary decrease of shrub *Alnus* precisely mirror millennial-scale climatic variations primarily known from Greenland ice-cores as Dansgaard-Oeschger cycles, as well as Late-glacial period climate changes. Percentages of trees & shrubs pollen and in particular lake productivity-related data reveal substantial differences between interstadial intensities, with those between 50 and 60 ka BP being more pronounced than the following ones.

1. Introduction

The East Asian monsoon, as an integrated part of the global monsoon system (Cheng et al., 2012) affects roughly one third of the world's population. In a traditional and simplified way, development of monsoonal systems has been explained with thermal land – sea contrast, leading to a strong pressure gradient with transport of warm humid air masses from high pressure oceanic regions to low pressure continental areas. Of course, in reality the monsoonal system is much more complex, with interactions with numerous factors such as surface and upper tropospheric flow patterns, sea surface temperature, El Niño and La Niña Southern Oscillation modes, land surface conditions like the Eurasian snow cover (Domrös and Peng, 1988; Chou, 2003; Wang, 2006). Particularly the cyclonic activity during summer in Northern China is strongly influenced by the West Pacific Polar Front (Barry and Chorley, 1998). The main source of precipitation, however, lies in the south, as a study of air mass transport pathways in northeast China from 1961 to 2002 revealed (Sun et al., 2007). The ongoing climate change affects the regions of East Asia differently, with serious economical consequences (e.g. Yang et al., 2007).

To understand the current and foresee the future climatic variability, expected to show changed amplitudes and dynamics but with still large uncertainties in projections (e.g. Bony et al., 2013; Cai et al., 2014), requires time series of climate variability beyond the reach of instrumental and historical data. Numerous palaeoclimate archives with different proxies from loess deposits (e.g. Lu et al., 2007; Sun et al., 2012), caves (e.g. Wang et al., 2001, 2008; Zhou et al., 2008), lake sediments (e.g. Yancheva et al., 2007;

* Corresponding author.
E-mail address: jens.mingram@gfz-potsdam.de (J. Mingram).

https://doi.org/10.1016/j.quascirev.2018.09.023
0277-3791/

Stebich et al., 2009, 2015; Nakagawa et al., 2012), peat bogs (e.g. He et al., 2015) and marine sediments (e.g. Nagashima et al., 2007, 2011) have been investigated to understand the Glacial-Interglacial and millennial-scale East Asian Monsoon variability.

In particular, stable isotope records from speleothems came into focus due to their apparent direct relation to monsoonal climate parameters and inherent possibility of annual layer counting plus independent radiometric dating. However, the use of stable oxygen isotope data from Chinese speleothems as a proxy for the on-site intensity of the East Asian Summer Monsoon (EASM) intensity (Wang et al., 2001) has been increasingly challenged by recent research (e.g. Maher and Thompson, 2012). However, after having been initially linked to the local summer monsoon intensity (Wang et al., 2001), the use of stable oxygen isotope data from caves of the Chinese mainland as an East Asian Summer Monsoon (EASM) proxy has been increasingly called into question (e.g. Maher and Thompson, 2012). Modern precipitation- and speleothem isotope data are not matching spatially, and possibly Chinese cave deposits reflect changes in vapour sources and/or monsoon variability upstream of the cave sites (Johnson and Ingram, 2004). The picture is even more complicated if, in addition to cave stable oxygen isotopes, also carbon isotopes are considered. At least most authors agree that speleothem carbon isotopes mirror local effective moisture – mediated mainly by local vegetation and soil conditions (Liu et al., 2016). In general speleothem oxygen isotopes seem to reflect millennial- and precession-scale variability and a so-called "mean status" of the monsoon, whereas carbon isotopes could reflect centennial, decadal and even seasonal variability (e.g. Liu et al., 2016). A recent modelling study by Liu et al. (2014) offers a plausible link of speleothem data with the EASM variability, namely southerly wind intensity and precipitation in northern China.

Apparent similarities in millennial-scale signal variability between the Last Glacial North Atlantic atmospheric system (as evidenced most prominently from Greenland ice cores) and the East Asian monsoon (as shown most prominently from speleothems) climate records have stimulated research to understand the mechanistic links between them (Wang et al., 2001; Vandenberghe et al., 2006; Liu et al., 2010; Shen et al., 2010; Duan et al., 2018). The large monsoonal picture might be controlled by meridional shifts of the intertropical convergence zone (ITCZ), which could originate in interlinked changes of northern meltwater discharge, Atlantic meridional overturning circulation (AMOC) and northern sea ice coverage (e.g. Cheng et al., 2012). Initiated by investigations of e.g. Schiemann et al. (2009) and Nagashima et al. (2011), a more prominent role of the Westerlies in triggering East Asian monsoonal changes has been highlighted. Starting from modern observations of the interplay between the Westerly jet and the seasonal northward propagation of the EASM (Chiang et al., 2015) developed a hypothesis to explain the millennial-scale variability of speleothem isotope signatures and the behavior of the palaeo-EASM. Central to their discussion is the position of the Westerlies south or north of the Tibetan Plateau, which in extreme cases of cold stadials may have rested south, blocking the northward monsoonal air flow.

Here, we present results from a long, laminated sediment profile obtained from a lake in NE-China. The main focus of this paper is on the variability of the East Asian Monsoon, both summer and winter, from a site close to the NE-limit of the EASM front. Compared to other natural climate archives lake sediments offer the advantage of a broad range of palaeoenvironmental and palaeoclimatic parameters. The challenge with lake sediments is to discriminate local from regional signals, and to recognize and interpret thresholds of the lake system. Besides providing a large variety of environmental and climate proxy parameters, especially annually laminated (varved) lake sediments have the advantage of independent and precise timescales which is the main prerequisite for regional and hemispheric correlation of climate archives, and finally for understanding of the functioning of the climate system (Zolitschka et al., 2015).

2. Study area and investigated site

The Long Gang Volcanic Field (LGVF), Jilin Province, N.E. China (Fig. 1a and b) is morphologically dominated by 148 volcanic cones and craters distributed on a plateau-like surface at an altitude of approximately 600 m above sea level. Nine of the volcanic structures are water-filled and form the so-called Long Wan Lake District.

Rocks belong to the Upper Archaean Anshan migmatite group with mainly acidic granitoids and the Quaternary Long Gang Volcanic Group with predominantly alkali-basaltic rocks form the catchments of the lakes (Liu, 1988; Liu et al., 2000a; b; Liu et al., 2001).

The climate of the LGVF is characterized by strong seasonal contrasts both in temperature and precipitation. Winters are cold and dry, dominated by north-westerly winds. The region is under the track of moving dust clouds from the Asian interior towards the Pacific Ocean with a maximum dust flux reached in spring (Littmann, 1991). Warm and moist air masses from the Pacific dominate the summer with maximum precipitation in July and August. Recent temperature records of the meteorological station nearest to SHL (Jingyu town) show mean July (January) values of +20.7 (−18.1) °C for the period AD 1955–1997, the mean annual temperature is 2.9 °C (Schettler et al., 2006c).

The LGVF belongs to the temperate mixed conifer and broad-leaved deciduous forest region (Liu et al., 1999; Sun and Chen, 1991; Sun et al., 1991), dominated by different species of *Pinus*, *Picea*, *Acer*, *Juglans*, *Quercus*, *Ulmus*, and *Fraxinus*. Noticeable anthropogenic influences in the study area are restricted to the last centuries only (Liu et al., 1999; Ren, 2000). At present, two *Alnus* species are also common in the Longgang and Changbai regions, *Alnus hirsuta* and *Alnus fruticosa* var. *mandshurica* (Atlas of woody plants in China, 2009). Especially the latter, a shrub, is adapted to inhospitable climatic conditions. *Alnus fruticosa* is the dominant species of *Alnus* on permafrost in northern Siberia (Tarasov et al., 2005). This shrub needs habitats not much shadowed by other trees and has abilities to grow on raw soils as a pioneer species due to a symbiosis with nitrogen-fixing bacteria. Almost all *Alnus* pollen found in Last Glacial SHL samples are from shrubs, hence if referred to *Alnus* later on it is always *Alnus* (shrub). More thermophilous tree species such as *Ulmus* and *Fraxinus* are typical elements of temperate cool mixed forests (Prentice et al., 1996). Different species of both genera are presently distributed in NE China, *Ulmus pumila*, *Ulmus macrocarpa* and *Ulmus laciniata*, as well as *Fraxinus mandshurica* and *Fraxinus rhynchophylla* (Atlas of woody plants in China, 2009). At higher northern latitudes both genera are ecologically more associated with humid sites and slopes near rivers at altitudes between 700 and 2500 m a.s.l. (see Tarasov et al., 2005 for *Ulmus pumila* in S-Siberia).

Artemisia, a typical representative of cold/dry steppe communities in modern northern Eurasia (Prentice et al., 1996; Tarasov et al., 2000; Müller et al., 2010), stays for more dry, cold, weak-(summer)monsoon conditions in NE China.

After initial studies of several volcanic lakes of the LGVF, Lake Sihailongwan (SHL, Fig. 1c) was chosen for a long sediment record to investigate the main palaeoenvironmental and palaeoclimatic changes back into the Last Glacial (Liu et al., 2000a; b; Mingram et al., 2004).

SHL is a dimictic maar lake with a well-developed summer thermocline at a depth of c. 10 m (Mingram et al., 2004; Chu et al.,

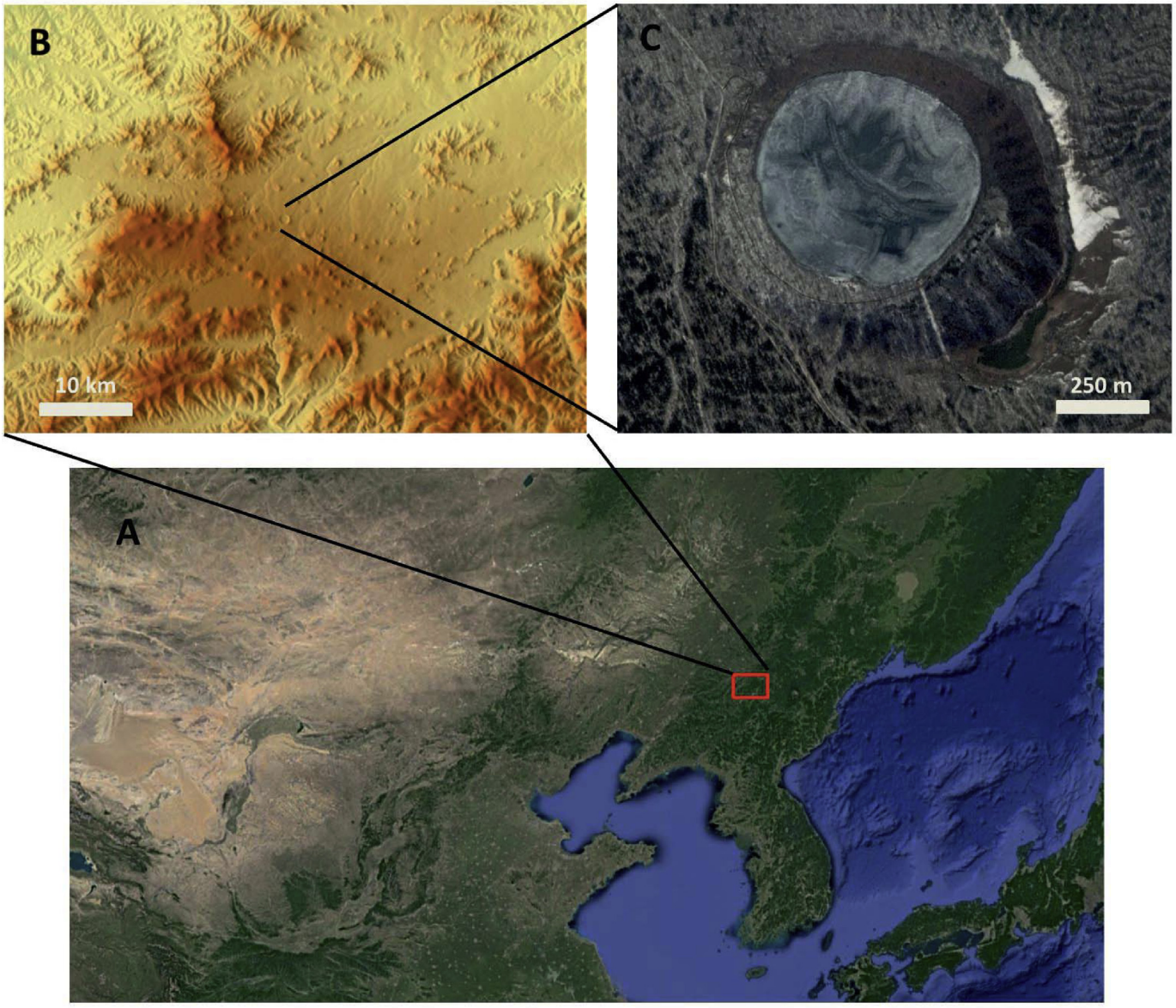

Fig. 1. Investigation area and site. (a) Satellite view of north-eastern China, red square – Longgang Volcanic Field (image from Google earth). (b) Longgang Volcanic Field and surroundings with relief contrast from SRTM digital elevation data (image from www.deine-berge.de). (c) Lake Sihailongwan with ice cover in spring (image from Google earth, satellite image taken on 26th of March, 2014). (For interpretation of the references to color in this figure legend, the reader is referred to the Web version of this article.)

2005). Maximum water depth of the lake is about 50 m; the catchment comprises only the interior of the maar crater rim and rises up to about 120 m above the lake surface.

Temperature reconstructions revealed that summers in northern and central Asia were 1–7 °C colder than recent during the Last Glacial Maximum (LGM) (Tarasov et al., 1999), and winter temperatures in NE-China were higher than recent during the middle and early Holocene (Ren and Beug, 2002), but reconstructed mean temperature of the coldest month, even when considering the upper uncertainty limits, were never at or above the freezing point (Jiang et al., 2006). Consistently, the recent seasonal succession with a permanently ice-covered lake in winter and an ice-free lake in summer should have been in place during the whole Holocene and the Late-glacial period as well as during Last Glacial stadials and interstadials and even during the LGM.

Hydrochemical modelling clearly shows balancing of the lake via precipitation-controlled groundwater. Autochthonous productivity is limited by phosphorus availability in the photic zone. An enhanced net accumulation of biogenic silica in Holocene sediments compared to Last Glacial sediments is sustained by soluble reactive phosphorus (SRP) and dissolved silicate (DSi) influx via groundwater discharge from the catchment (see hydrochemical data for chemical stratification of the modern lake and the groundwater inflow from the lake's catchment in Schettler et al., 2006a). The catchment of SHL and modern SHL sediments are non-calcareous. Significant influx of carbonate (of remote origin) only occurred during high dust periods (as e.g. the Late Pleniglacial and the Younger Dryas, see Fig. 2f in Schettler et al., 2006c) as direct fallout or inwash from dust-enriched soils of the catchment. Hence, the siliciclastic sediment fraction is dominated by aeolian input of remote provenance (Schettler et al., 2004; Schettler et al., 2006a; Zhu et al., 2013). For the Holocene the siliciclastic sediment fraction amounts to about 75 weight-% of the total sediment, and contributions from local alkalibasaltic debris are generally minor

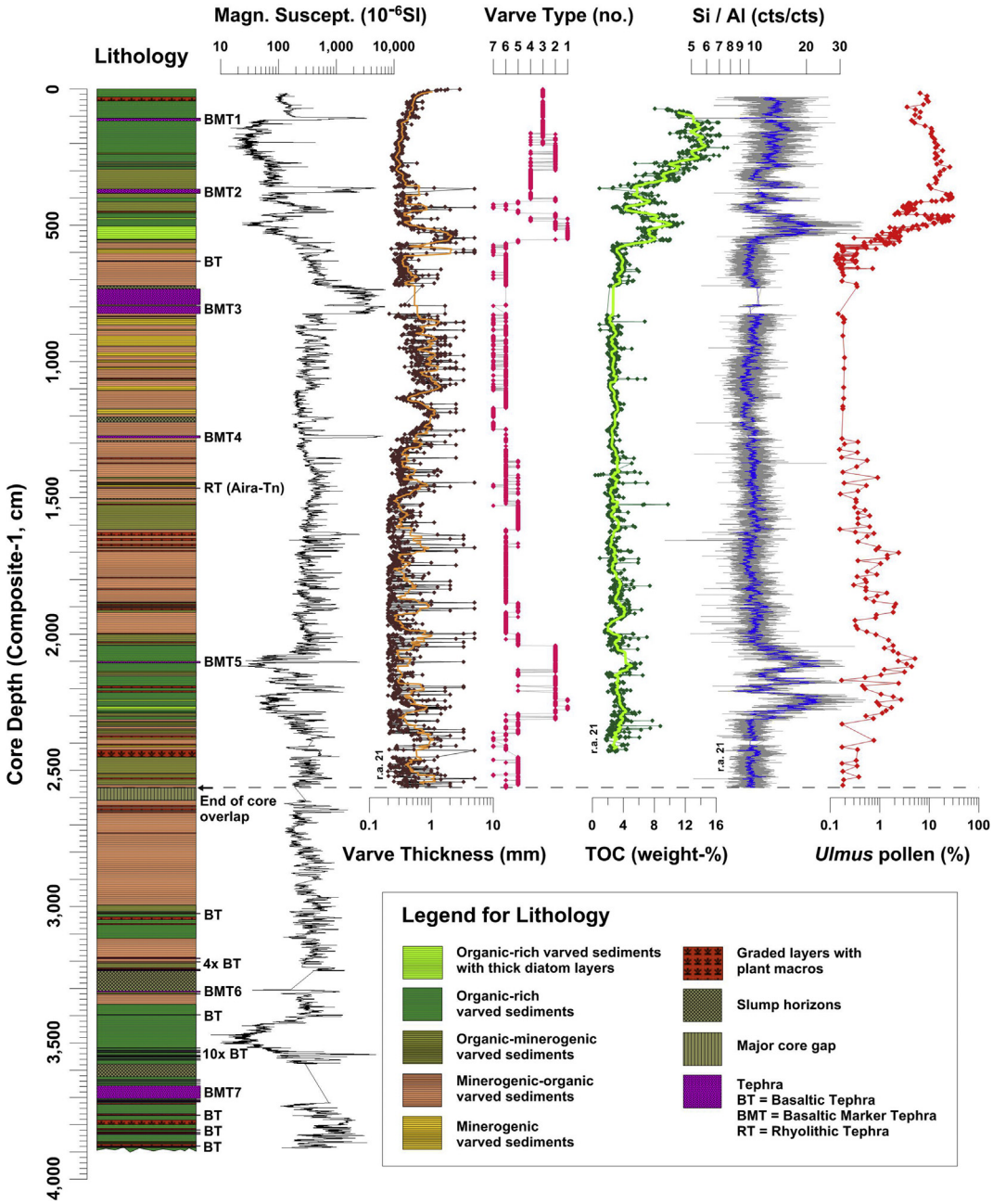

Fig. 2. Lithological profile of Lake Sihailongwan sediments with selected data against core depth. Magnetic susceptibility data shown for the entire profile, all other data downcore until the end of overlap of at least two coring sites (r.a. 21 = running average over 21 data points). Note: smaller changes in lithology as well as small tephra and smaller core gaps below the end of overlap are not shown.

(Schettler et al., 2006a).

High resolution pollen studies suggest close links of the climatic development in the Late-glacial period between NE-China, Western Europe and Greenland, with a pronounced climatic deterioration at SHL parallel to the Younger Dryas (YD)/Greenland-Stadial I, and another, shorter, climate deterioration phase parallel to the Gerzensee fluctuation/Greenland-Interstadial I b (Lotter et al., 1992; Björck et al., 1998; Stebich et al., 2009).

3. Materials and methods

3.1. Coring, core correlation and subsampling

In 2001 three overlapping cores were recovered from the centre of SHL (Fig. 1c) at a water depth of 50 m with the Usinger piston coring system (Mingram et al., 2007). The lengths of the parallel sediment cores were 38.9 m (SHL-A), 22.7 m (SHL-B), and 16.7 m (SHL-C). Undisturbed surface sediments were already recovered in 1998 and 1999 with gravity corers and a liquid nitrogen freeze-corer (Schmidt et al., 1995). All core barrels were kept in cold conditions during field storage and transport. Immediately after opening at GFZ Potsdam laboratories the cores were split into a working and an archive half, described visually, photographed and scanned using a GEOTEK line scan camera. Sediments were finely laminated throughout, allowing the creation of a composite master profile (Composite-1) using best preserved parts from all three overlapping cores on the basis of high-resolution prints of the core photos and additional magnetic susceptibility measurements

(Fig. 2). Samples for 10 cm long overlapping petrographic thin sections, covering the whole Composite-1, and samples for pollen analyses have been taken from the working half of Composite-1 profile, whereas samples for geochemical analyses were taken from overlapping cores of Composite-2 profile in order to keep an undestroyed Composite-1 archive half core for any kind of non-destructive measurements. All discussions and the age model presented in this paper are restricted to the uninterrupted part of the profiles down to a Composite-1 depth of 25.63 m (Fig. 2). Downcore from 25.63 m there is only one core (SHL-A) available, with cm-scale gaps between the individual core sections.

3.2. Radiocarbon dating

In addition to the previously published ^{14}C dates of SHL Holocene and Late-glacial period sediments (Schettler et al., 2006c; Stebich et al., 2009) we got new radiocarbon ages from 7 samples (4 woody remains, 2 mosses, 1 mixed sample) of the Last Glacial. Two more samples have been out of the range of the radiocarbon calibration curve. To calibrate our new and re-calibrate the former AMS ^{14}C dates the IntCal13 Northern Hemisphere atmospheric radiocarbon calibration curve (Reimer et al., 2013) has been applied. Calibrations of AMS ^{14}C ages have been performed using the programme Calib 7.1 (Stuiver et al., 2017) (Table 1).

3.3. Geophysical data

All split cores have been scanned for magnetic susceptibility with an automated logger (GFZ automated logging system equipped with a Bartington Instruments® surface scanning sensor MS2E/1) with a step width of 1 mm. Decrease/increase in magnetic susceptibility values of lake sediments could be caused by decrease/increase of minerogenic clastic influx and/or longer/shorter lasting conditions with oxygen depletion in the deep water and higher H_2S production in the surface sediments causing subsequent diagenetic dissolution of magnetic carriers (Nowaczyk et al., 2007). Here we use magnetic susceptibility data to distinguish organic-rich and organic-poor sediments for the composite profile.

3.4. Geochemical data

Contents in total organic carbon (TOC), total nitrogen (TN), and CO_3 for the Last Glacial were measured at a 1-cm sampling resolution from Composite-2 profile and following the methods described in Schettler et al. (2006c).

Inorganic carbon has been estimated as described in Schettler et al. (2006a) and calculated as CO_3-equivalents.

The Si/Al ratio of the whole profile has been determined from Si and Al data (cps) generated with a micro X-ray fluorescence (μ-XRF) spectrometer EAGLE BKA (Röntgenanalytik Messtechnik GmbH, Germany) from split cores of Composite-1 profile. A detailed description of the instrument is presented by Haschke (2006). The instrument was equipped with a Rh-X-ray tube, a capillary lens system to focus the X-ray beam onto the sample and a Si(Li) semiconductor detector. To minimize the absorption of the fluorescence radiation of light elements (e.g. Al, Si), the space between sample surface and detector window was flushed with Helium. For single-line measurements tube voltage was set to 40 kV, tube current to 400 μA and dwell time to 30 s. The applied resolution was 500 μm resulting in 2000 points per meter.

3.5. Palynological data

Preparation of pollen samples has been performed following standard methods described in Berglund and Ralska-Jasiewiczowa (1986). *Lycopodium* spores were added to each sample for calculation of pollen concentrations. Pollen percentages were calculated on the basis of terrestrial pollen, excluding aquatics, telmatics, and spores. The sampling resolution is typically 10 cm, except for the pollen of Late-glacial period sediments that were counted at 1–2 cm; all pollen samples are from Composite-1 profile. Shown and discussed are only total arboreal pollen data and some selected taxa (*Ulmus*, *Fraxinus*, *Alnus*, *Artemisia, Betula*) which exhibit strong sensitivity to the last glacial monsoon variability.

3.6. Sediment microfacies analysis, diatoms and varve counting

More than 300 large thin sections (each comprising 10 cm of sediment) from freeze cores, gravity cores, and piston cores were prepared using the freeze-drying technique described in Werner (1966) and Merkt (1971). All thin sections were scanned with a transmitted-light flatbed scanner equipped with polarizing foils to create a low-magnification "working diary", contrasting especially minerogenic layers, for the entire master profile. To deduce various minerogenic and organogenic sediment components different microscopic techniques were applied, in detail plane polarized/crossed polarized light for minerogenic and organogenic components, and dark field illumination and fluorescence (with broadband incident blue light excitation) for some organogenic constituents. Identification of diatoms is based on scanning electron microscope (SEM) photos taken from dried and freshly broken samples of all lithotypes. Some samples were also examined for diatoms under the light-microscope using conventional techniques for slide preparation (e.g. Battarbee et al., 2001). Diatom species were identified using a large number of taxonomic references as well as standard floras (Hofmann et al., 2011; Metzeltin et al., 2009).

Varve counting has been performed on 10 cm-long overlapping thin sections from Composite-1 for 1 cm increments. Transfer of core depths to depth scale of thin sections has been done using a transmitted light box for diapositives. Thin sections were placed between polarizing foils on the light box, and core photos printed at 1:1 scale and illuminated separately from above were held aside for correlation of marker layers and fine lamination features. Thus, precise varve ages have been assigned to each core with 1 cm resolution. An index of varve quality as well as the number and thickness of graded layers were estimated at a 1-cm resolution from thin sections. Varve thickness data have been calculated based on varve numbers of 1 cm Composite-1 section increments, not considering graded event layers and tephra.

4. Results and discussion

4.1. Sediment composition

The whole SHL profile consists of nearly continuously laminated lake sediments with intercalated seven major (between 3 and 57 cm thick) and numerous minor (single grain to mm – sized) tephra layers (Fig. 2).

Major sediment components can be roughly divided into (A) allochthonous minerogenic matter (feldspar, quartz, clay minerals, minor amounts of mafic minerals, volcanic rock clasts and pumice), (B) autochthonous (diatoms, chrysophyte stomatocysts and -scales, *Daphnia* resting eggs, and rare sponge spicules), and (C) allochthonous biogenic particles (mainly terrestrial plant remains). Minor amounts of carbonate (as detected from thin section microfacies analyses so far only siderite) and vivianite are most probably of early diagenetic origin. According to the classification scheme after Troels-Smith (1955), SHL sediments vary between diatomaceous gyttja (Lso3Ld1As) representing the high-organic "end member"

Table 1
Lake SHL sediment radiocarbon ages and corresponding varve ages. Leaf* - too less material for dating, sample not considered. Sample Poz-10361 no 2-Sigma lower limit available,** - sample not considered for age model. Sample Poz-5437 – out of CALIB 7.1 calibration range. Data from shaded boxes in SHL-A, SHL-B, SHL-C profile depth rows belong to Composite-I profile. Data in bold from SHL-A, SHL-B, SHL-C profile depth rows indicate samples for radiocarbon dating from this particular profile; other depths have been correlated.

Sample Depth at Comp. I Midpoint (cm)	Lab. Code	Btm. in SHL-A	Btm. in SHL-B	Btm. in SHL-C	Varve Age (before 1950) at sample midpoint	Sample Type	CALIB 7.1 2 Sigma upper limit	CALIB 7.1 2 Sigma lower limit	Median Probability	Difference between CALIB 7.1 Median Probability and Varve Age before 1950	shl-vc2 age
	KIA 8097		1-u 29		633	leaf	511	624	536	-97	670
	KIA 8098		1-u 31		669	leaf	309	478	390	-279	708
77,50	AA 60290	1-o 62,5	gap	**C1-o 78**	1289	wood	1179	1299	1249	-40	1364
97,00	AA 60291	1-o 82	disturbed	**C1-u 2**	1741	leaf	1574	1821	1706	-35	1842
98,00	Poz-5432	**1-o 83**	disturbed	1-u 3	1761	leaf	1556	1710	1635	-126	1864
118,80	AA 60292	1-u 5	2-o 25,8	**1-u 20**	2063	leaf	1993	2304	2109	46	2183
128,00	Poz-10349	1-u 14,8	**2-o 35**	1-u 27	2345	leaf	2360	2703	2527	182	2482
147,00	AA 60293	**1-u 34**	2-o 54	1-u 41,4	2889	leaf	2930	3207	3061	172	3057
163,00	AA 60294	**1-u 50**	2-o 70	1-u 49,3	3372	leaf	3459	3717	3603	231	3568
165,30	Poz-5429	1-u 51,8	**2-o 71,8**	gap	3456	leaf	3592	3848	3731	275	3657
172,20	Poz-10377	1-u 58,8	**2-o 79,2**	gap	3658	leaf	3891	4085	3977	319	3871
178,50	AA 60295	**1-u 65**	**2-o 85,5**	gap	3848	leaf	4161	4511	4342	494	4072
186,50	Poz-10378	1-u 72,7	**2-o 93**	2-o 14	4071	seed	4440	4809	4578	507	4308
194,50	Poz-5430	**1-u 80,5**	2-o 101	2-o 21	4330	seed	4577	4835	4711	381	4582
194,50	Poz-5431	**1-u 80,5**	2-o 101	2-o 21		leaf*					
198,50	AA 60296	disturbed	**2-u 3**	2-o 25,7	4457	leaf	4840	5272	4953	496	4717
214,10	Poz-10350	2-o 21,7	**2-u 18,7**	2-o 40,1	4999	leaf	5328	5586	5510	511	5290
225,40	Poz-10351	2-o 33	**2-u 29,9**	2-o 49,6	5370	leaf	5715	5911	5816	446	5683
237,80	AA 60297	2-o 43,3	2-u 42,3	**2-o 61**	5774	leaf	6299	6479	6379	605	6110
251,50	Poz-5428	2-o 56	2-u 56	**2-o 74**	6294	leaf	6743	7001	6875	581	6661
262,50	AA 60304	2-o 65	2-u 67	**2-o 84**	6701	leaf	7014	7318	7208	507	7091
290,00	AA 60305	**2-o 89**	2-u 94,6	2-u 5	7625	leaf	8046	8373	8238	613	8069
306,90	Poz-10352	2-u 2,1	**3-o 5,4**	2-u 22	8243	leaf	8650	9007	8860	617	8723
318,50	AA 60298	**2-u 14**	3-o 17	2-u 33,3	8585	leaf	9156	9885	9510	925	9085
357,00	Poz-10368	2-u 53,5	3-o 55,5	2-u 71,5	9662	seed	10234	10500	10350	688	10225
362,80	AA 60299	**2-u 60**	3-o 61,3	2-u 78	9832	leaf	9936	10411	10224	392	10405
385,75	Poz-10344	**2-u 87,7**	3-o 84,1	gap	9994	moss	10767	11202	10989	995	10576
386,00	Poz-10353	2-u 88,2	**3-o 84,5**	gap	9997	leaf	10742	11143	10937	940	10580
408,90	AA 60303	3-o 46,8	3-u 17,4	**3-o 27**	10604	seed	11217	11617	11357	753	11222
424,30	AA 60300	3-o 62,5	3-u 32,8	**3-o 42**	11033	wood	11653	12381	11977	944	11676
451,75	Poz-5434	**3-o 90,5**	3-u 60,5	3-o 70	11573	moss	11628	12384	11970	397	12247
465,60	Poz-10354	3-o 104,2	**3-u 74,2**	3-o 84,1	11979	leaf	12703	12980	12799	820	12677
466,70	AA 60301	3-o 105,6	3-u 75,2	**3-o 85**	12012	leaf	12659	13127	12878	866	12712
481,00	AA 60302	3-u 17,6	3-u 89,5	**3-o 102**	12336	leaf	12564	12935	12727	391	13055
565,00	Poz-10355	4-o 58,9	**4-u 70**	4-o 72,5	13430	moss	14043	14786	14354	924	14213
615,20	Poz-10346	**4-u 11**	5-o 17,7	4-u 18,7	14392	wood	15753	16207	15982	1590	15231
662,25	Poz-10362	4-u 61	5-o 67	**4-u 66**	15695	moss	16020	16893	16419	724	16610
703,00	Poz-10364	gap	5-u 8	**5-u 19,5**	16665	moss	17807	18229	18006	1341	17636
834,50	Poz-10365	5-u 32,5	6-o 42	**6-u 19**	17569	moss	18876	19316	19076	1507	18593
890,20	Poz-5438	5-u 88,5	**6-o 97,2**	gap	18422	needle	18022	19102	18596	174	19495
1173,50	Poz-5435	**7-u 88**	8-o 86	10-o 80,5	22415	needle	23038	23712	23398	983	23721
1345,50	Poz-10366	8-u 64	gap	**11-u 64**	24934	wood	27157	27683	27433	2499	26387
1354,50	Poz-5436	**8-u 73**	10-u 11	11-u 73	25241	moss	26411	27246	26836	1595	26712
1527,00	Poz-10356	11-u 30,5	**11-u 30**	12-u 24	29905	wood	31067	32403	31542	1637	31648
1654,00	Poz-10348	**12-o 74**	12-o 68	13-u 60,5	34018	wood	35112	37175	36102	2084	36000
1655,50	Poz-10358	12-o 76	**12-o 70**	13-u 62,5	34018	moss	34153	36474	35328	1310	36000
1655,50	Poz-10359	12-o 76	**12-o 70**	13-u 62,5	34018	mixed	34839	36458	35684	1666	36000
1723,00	Poz-10360	12-u 38,1	**12-u 32**	no core	35864	wood	36365	38447	37411	1547	37954
1999,50	Poz-10361	14-u 2	**14-u 21**	no core	46044	wood	45179	none	47703	1659**	48727
2157,50	Poz-5437	**15-u 58,5**	15-u 87,5	no core	52036	moss	none	none	none	none	55068

and clayey silt (Ag3As2) without any autochthonous organic matter as the minerogenic "end-member".

4.1.1. Varves

The varved nature of the laminated SHL sediments has been documented by sediment microfacies investigations and AMS ^{14}C – dating (Mingram et al., 2004), sediment trap data (Chu et al., 2005), ^{210}Pb and ^{137}Cs measurements (Schettler et al., 2006b), and additional microfacies analyses presented here.

Varves of modern SHL sediments are of mixed organogenic-minerogenic origin with a clastic spring melt layer as the most prominent feature, followed by a mixed layer resulting from both allochthonous (minerogenic particles and terrestrial plant remains) and autochthonous components (mainly lake biota like diatoms, chrysophytes, green algae) and a thin diatom layer composed mainly of *Discostella pseudostelligera* (synonym = *Cyclotella pseudostelligera*) directly beneath the next clastic spring layer (Mingram et al., 2004).

Concordant with thin section observations, sediment trap data revealed the highest flux of both minerogenic and organic matter in

spring, whereas the minerogenic flux during the rainy summer period is low. High biogenic silica flux has been observed in spring, and again from late summer until late autumn (Chu et al., 2005). The biogenic silica maximum in autumn postdates the precipitation maximum by ca. 2 months, which could be related to delayed influx of nutrient-rich groundwater into the lake and/or settling time of diatoms. An alternative explanation is that this second peak in biogenic silica is related to the ecology of diatoms associated with the autumn bloom (e.g. *Lindavia* sp.), as these large-cell diatoms take advantage of the seasonal mixing of the water column to remain in suspension within the epilimnion.

Studies from numerous lakes of the Northern temperate zone revealed similar successions with pronounced, mostly allochthonous-minerogenic spring melt layers, followed by mostly organogenic deposits during summer and autumn, and fine-grained or even amorphous winter layers formed at still-water conditions under lake ice (Renberg, 1982; O'Sullivan, 1983). Warm season surface runoff from forested catchments of small temperate lakes is considered to be in general of minor importance compared to spring melt runoff (Wright, 1976; Nuhfer et al., 1993). Thin diatom layers beneath clastic spring layers have been interpreted as a result of autumn blooms assuming long settling time for diatoms under winter quiet water conditions (e.g. several months for 30 m deep Elk Lake, Bradbury, 1988).

The observed recent sedimentation pattern of SHL sediments results basically from the strongly seasonal climate of the region, with long-lasting lake ice cover in winter, a spring melt period with lake turnover, a much warmer, ice-free summer, and a second lake turnover period in autumn. Seasonal overturn, accompanied most probably with at least partly sediment oxygenation, occurs during spring and autumn. However, under recent conditions this obviously does not hamper varve preservation in the centre of the lake basin, probably due to high oxygen consumption by settling organic matter and longer anoxic conditions in the deep water. Gravity cores taken from a transect through SHL exhibited no varves in sediments from water depths above 26 m. Thus, the lake should have been deeper than approximately 26 m for all periods with well-preserved varves of similar microfacies, presuming a similar seasonal sedimentation contrast and a dimictic lake.

Resulting from the persistent and strong seasonal climate contrast of the study area with permanently ice-covered lake in winter, the most pronounced and stable seasonal sediment feature throughout the whole SHL sediment record is the spring silt layer. It is the result from direct input from the melting ice cover and surface runoff during and after snow melt. Other sublaminae like mixed diatomaceous/minerogenic layers, well sorted fine-grained minerogenic layers, diatom layers and layers of stomatocysts and chrysophyte scales are more variable, depending on changing climatic, ecological, and hydrological conditions.

Varves containing carbonate have been observed mainly during stadial periods, and carbonates are often associated with late autumn-, winter-, and spring layers. Wintertime bacterial activity in the sediment surface layer of temperate lakes is a major cause for oxygen depletion and may contribute an important part to overall autochthonous respiration (Ellis and Stefan, 1989; Sobek et al., 2006; Karlsson et al., 2008). As siderite is preferably precipitated under reduced oxygen or anoxic conditions in the hypolimnion (Berner, 1981; Wetzel, 2001), oxygen consumption by bacterial respiration during the long-lasting winter still-water period under ice could also favour winter carbonate layers.

Based on thin section investigations we define seven major varve types to describe and visualize lithological changes throughout the entire SHL sediment profile (Table 2, Figs. 3 and 4). Varve types are arranged from high to low numbers with increasing productivity (as defined mainly by the occurrence of diatoms in

Table 2
Lake SHL varve types. Descriptions based on thin section investigations using varying contrasting techniques (plane transmitted light, partly or fully polarized light, dark field illumination, incident-light fluorescence). Varve types arranged according to their content of autochthonous organic components as observed in thin sections (i.e. lake productivity; 1 – very high, 7 – very low). Troels-Smith code after Troels-Smith (1955).

No.	Type	Short Description of Varve Types	Troels-Smith code	Mean thickness (μm)	Occurrence
1	organic-minerogenic, diatom layer, high deposition rate	Minerogenic spring layer and extremely thick diatom spring and/or summer layers; large influx rates of both organic and minerogenic constituents; often vivianite concretions.	Lso Ld As	1200	start of the Late- glacial period, some warmer Interstadials
2	organic-minerogenic, spring diatom layer	Minerogenic spring layer followed by a thick diatom layer, then followed by a mixed clastic-organic summer layer.	Ld Lso	300	Late-glacial period, warmer interstadials, Holocene
3	organic-minerogenic, clastic spring + mix layer	Minerogenic spring layer, in recent varves followed by pollen accumulations, then a mixed layer. Fine-grained winter layer with tiny, but visible diatom layer, no diatom layer in spring or summer. Mean varve thickness is 500 μm due to lower compaction in the upper part, below 1 m mean varve thickness is 300 μm.	Ld Lso	500	late Holocene, recent
4	organic-minerogenic + dust layer	Minerogenic spring layer present, but not well expressed, followed by (sometimes alternating) diatom and mixed layers; then a well-sorted, silt-sized minerogenic (summer - autumn) layer, followed by a thin winter clay layer.	Ld Lso Ag	350	early- to middle Holocene
5	minerogenic-organic with diatoms	Clearly expressed minerogenic spring layer, followed by a mixed summer layer and a winter clay layer. Abundant, but mostly dispersed, diatoms, plus Chrysophyte cysts and -scales. During spring or summer event layers with reworked soil material may occur.	Ld Lso As Ag T	300	Last Glacial, mostly during stadials
6	minerogenic-organic without diatoms	Clearly expressed minerogenic spring layer, followed by a mixed summer layer and a winter clay layer. Abundant Chrysophyte cysts and scales, only very minor amounts of diatoms. During spring or summer event layers with reworked soil material may occur.	Ld As Ag T	400	Last Glacial, mostly during stadials
7	minerogenic	Almost purely minerogenic varves, graded from silt-sized spring layer to winter clay layer. Remains of limnic biota only cysts and scales of Chrysophytes.	As Ag	1800	Last Glacial Maximum, some stadials, Younger Dryas

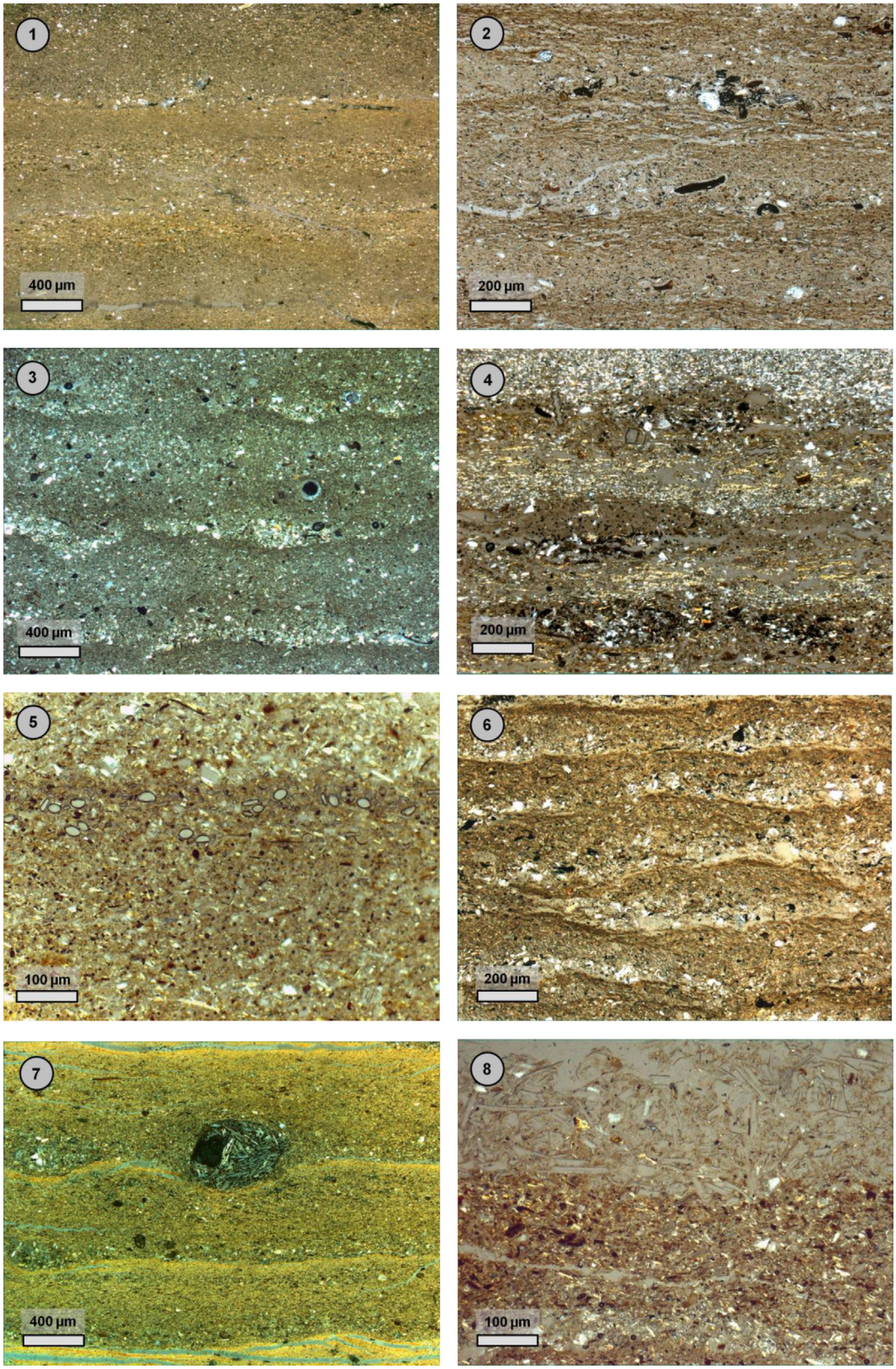

Fig. 3. Lake Sihailongwan varve types (1–7) shown as micro-photographs and Aira-TN tephra (8). All photos taken under transmitted light with partly crossed polarizing filters. Note different scales (shown lower left side at each photo). (1) Varve type 1 with thick varves and large amounts of diatoms. (2) Varve type 2 with less expressed minerogenic spring layer. (3) Varve type 3 with well-expressed minerogenic spring layer and a thin diatom layer underneath. (4) Varve type 4 with well-expressed minerogenic spring layer and a second, better sorted minerogenic layer probably originating from aeolian dust. (5) Varve type 5 with dominant minerogenic clastics plus mostly dispersed (but sometimes still layered as in the photo) diatoms and chrysophyte cysts. (6) Varve type 6 with very dominant minerogenic clastics and only rare occurrence of some autochthonous organics. (7) Varve type 7 composed entirely of thick clastic laminae, with pronounced winter clay layers and occasional occurrence of oversized dropstones (as in the centre of the photo). (8) Tephra layer of the Aira-Tn eruption (upper half of the photo), composed mainly of rhyolithic glass shards. The background sediment (lower half of the photo) is varves of type 6.

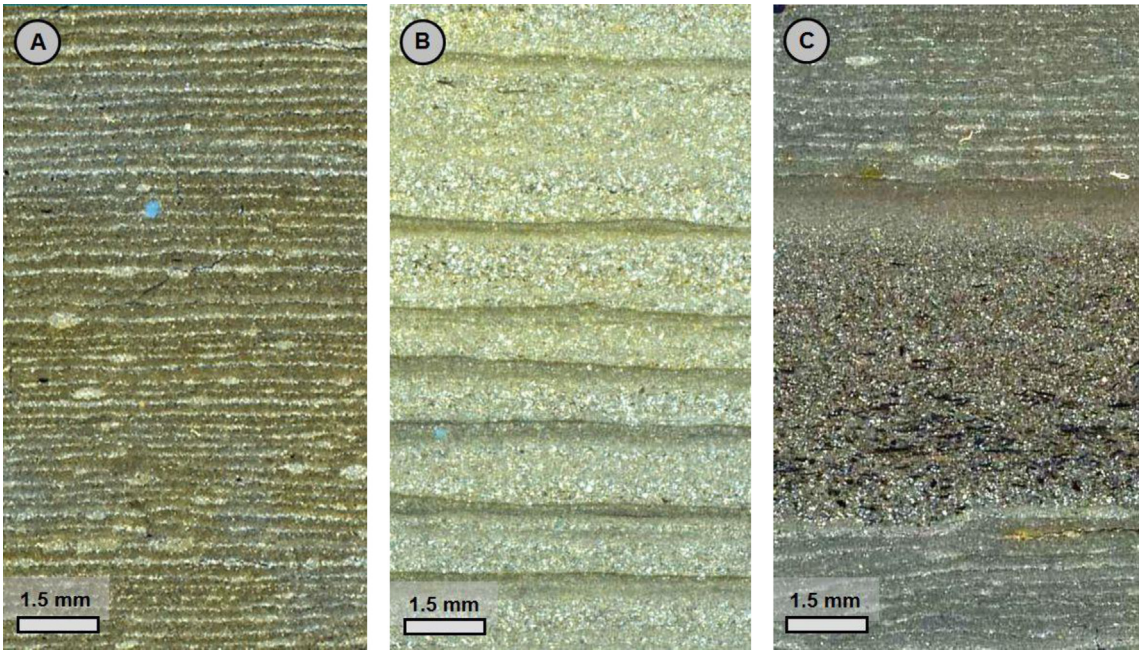

Fig. 4. Lake Sihailongwan laminated and graded sediment micro-photographs. (A) Regular, thin varves with pronounced clastic spring melt layer (brighter laminae). (B) Thick clastic-minerogenic varves of the Last Glacial Maximum. Darker laminae contain more clay and decomposed organic material deposited in winter. (C) Typical graded event layer (Type-I) with enrichment of reworked terrestrial plant macro fossils and siliciclastics. The layers show typical fining upward. Varves below and above the graded layer are same as in (A). All photos taken under transmitted light with crossed polarizing filters.

thin sections) with varve type 1 representing periods of highest productivity with thick seasonal diatom layers and varve type 7 as an almost purely minerogenic one.

Additionally to varve types we established six varve quality grades, from grade-1 representing undisturbed and perfectly preserved varves to grade-5 for nearly entirely homogenized lamination, and grade-6 for slumps. Varve quality estimates give a measure of varve counting reliability (Lotter and Lemcke, 1999) and may serve as a rough proxy for lake level changes as varves can be destroyed after lake level lowering by more intense mixing causing increased bioturbation. However, independently from water depth, varves can be influenced by water escape structures or early diagenetic disturbances due to density differences of minerogenic and biogenic sediment components. Varve thickness is determined by varying amounts of allochthonous and autochthonous components, in particular from spring snow melt, aeolian dust and diatom blooms. Hence, varve thickness can have similar values under completely different environmental conditions and must therefore always be discussed in conjunction with other parameters.

4.1.2. Graded event layers

Two graded event layers (Type-I and Type-II) are distinguished.

Type-I: Most common, and in particular during the Last Glacial, are brownish, graded event layers of mm to cm – scale with large amounts of reworked terrestrial plant debris (Fig. 4). They most probably indicate local soil inwash caused by precipitation events during the frost-free season due to reduced seepage for conditions with permanently frozen ground, and by higher erosion potential due to less dense vegetation cover. For the age model we calculated 1 year for all Type-I graded layers as there are often signs of small-scale erosion at the base.

Type-II: These layers do not contain larger amounts of visibly allochthonous components, but instead often exhibit a normal grading of laminated intra-clasts from internally reworked lake sediments. Type-II graded event layers are a major source of varve counting uncertainty due to the mix-up of in situ reworked material and material laterally transported from shallower parts towards the centre of the lake basin. For the age model we used a mean sedimentation rate interpolated from varved sediments above and below of Type-II graded layers.

4.1.3. Tephra layers

For the whole SHL sediment profile seven major (between 3 and 57 cm thick) marker tephra (MT-1 to MT-7) and more than twenty minor single-grains to mm-sized tephra layers have been identified. All thick marker tephra are of alkali-basaltic composition (Liu et al., 2009; Mingram et al., 2009, and unpublished data) and originate most probably from eruptions of local monogenetic volcanoes. As there is still a lack of available petrological data from local volcanic eruption centres except for the Jinlongdingzi Volcano (Fan et al., 1999), these tephra layers can serve firstly as correlation markers to other lake records of the LGVF where long sediment sections have been obtained (e.g. Lake Erlongwan – Frank, 2007; You et al., 2008; Lake Xiaolongwan – Chu et al., 2008; Liu et al., 2009). One of the thinner tephra layers has been already identified by means of microprobe glass-shard analysis and could be assigned to the Japanese Aira Volcano, providing an important tie point for the SHL chronology (see chapter below and Fig. 3). The occurrence of the Changbaishan Volcano "Millennium Eruption" tephra layer (e.g. Sun et al., 2015; Oppenheimer et al., 2017) in our SHL record has yet to be confirmed.

4.2. Chronology

SHL sediments are varved throughout, however, numerous mm – to cm-scale disturbances from lake-internal reworking and diagenetic effects like water escape structures or load marks due to large sediment density differences between seasonal layers make varve counting not a simple task. Some parts of the SHL profile have been counted by different investigators in order to estimate the

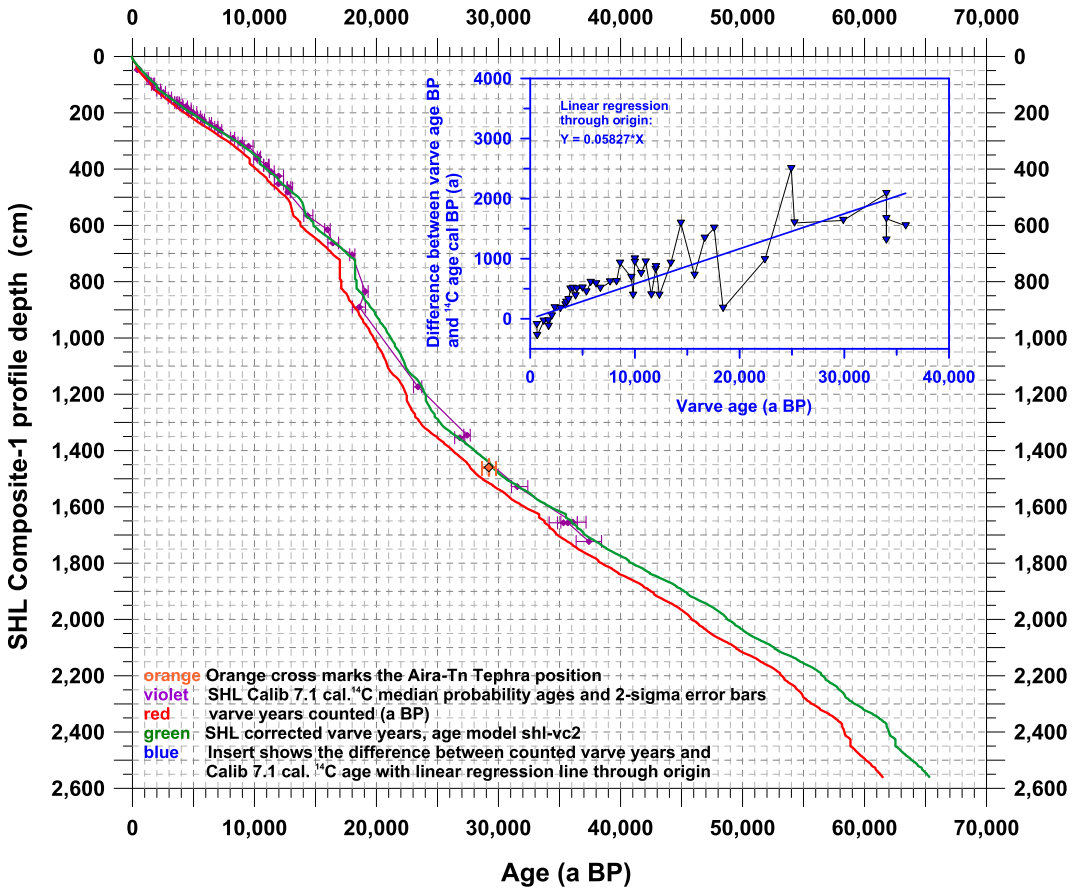

Fig. 5. Age model for Lake Sihailongwan sediments until the end of the composite profile with overlapping cores. The insert shows the difference between calibrated 14C ages and corresponding counted (uncorrected) varve ages of each 14C-dated sample. The regression factor derived from this graph has been used to correct SHL varve ages, resulting in shl-vc2 ages.

counting error. Double counts of several shorter Holocene and Last Glacial sections (with a total length of 2345 years) resulted in a total deviation of 39 years, whereas a continuous double count of a longer Last Glacial section of 9756 years resulted in a deviation of 663 years, or 6.8% (details are available as supplementary data with PANGAEA). Hence, the results call for an independent proof, and finally a correction, of the SHL varve chronology by ^{14}C dating (see e.g. Lotter and Lemcke, 1999; and Hajdas et al., 2000). A total of 50 samples have been dated by ^{14}C-AMS measurements (Table 1). The majority (40) are leafs of higher terrestrial plants, mosses, and seeds; 10 samples originate from small woody twigs. Incremental varve counts of SHL sediments are found to be systematically younger than corresponding ^{14}C-AMS dates. As a general rule, most varve counts of long sediment sections yield minimum chronologies. There are basically two different methods to correct for this deficit: applying a constant correction factor or, in case of disturbances by single events, adjusting with a local correction (Tian et al., 2005). For Lake Sihailongwan there is a more or less continuously increasing discrepancy between varve and calibrated radiocarbon ages with depth. Therefore, we applied a constant correction factor to transfer the counted varve ages into "corrected varve ages" which has the advantage of avoiding the accumulation of absolute age uncertainties from varve counting. A factor of 1.0622 has been estimated formerly from the slope of a linear regression line between counted varve ages BP and their difference with calibrated ages BP from AMS ^{14}C dating using Intcal 04 (Reimer et al., 2004). This factor has been applied for the SHL age model used in Schettler et al. (2006c), Stebich et al. (2009, 2015), and Zhu et al. (2013). Due to the new radiocarbon calibration (IntCal13, Reimer et al., 2013) and incorporation of some new ^{14}C dates the correction factor changed from 1.0622 to 1.05827 (Fig. 5), resulting in slight differences in absolute ages compared to the formerly used SHL age model. According to the updated age model, the onset of Late-glacial period conditions as set to 14.45 cal ka BP in Stebich et al. (2009) appears to be about 50 years later (younger) now. Varve counts for sediments older than the range of IntCal13 have been adjusted with the same correction factor (1.05827) based on the observation that there are no systematical changes in lamination type and -disturbances. Consequently, all SHL ages given in this paper are calendar ages before present (BP, i.e. 1950 AD) based on corrected varve counts; the chronology is referred now to as "shl-vc2". All cited ages from references are given on their reported base if not stated otherwise.

An independent proof for the Last Glacial chronology comes from a thin rhyolithic glass tephra at 14.64 m profile depth (Figs. 3–7). Microprobe analyses of glass chards yield chemical signatures identical with the Japanese Aira-Tanzawa (Aira-Tn) tephra (Mingram et al., 2009; details are available as supplementary data with PANGAEA) which has been dated at 25,120 ± 270 ^{14}C a BP (Miyairi et al., 2004). The shl-vc2 age of 29,627 a BP for this tephra is within the 2-sigma error range of the calibrated Aira-Tn age (2-sigma range 28.577–29.831 cal ka BP, median probability 29.173 cal ka BP with IntCal13, Reimer et al., 2013), hence the Aira-Tn corroborates the SHL chronology (Fig. 5). Moreover, it provides an important regional chrono-marker bridging the East Asian mainland with the Japanese arc.

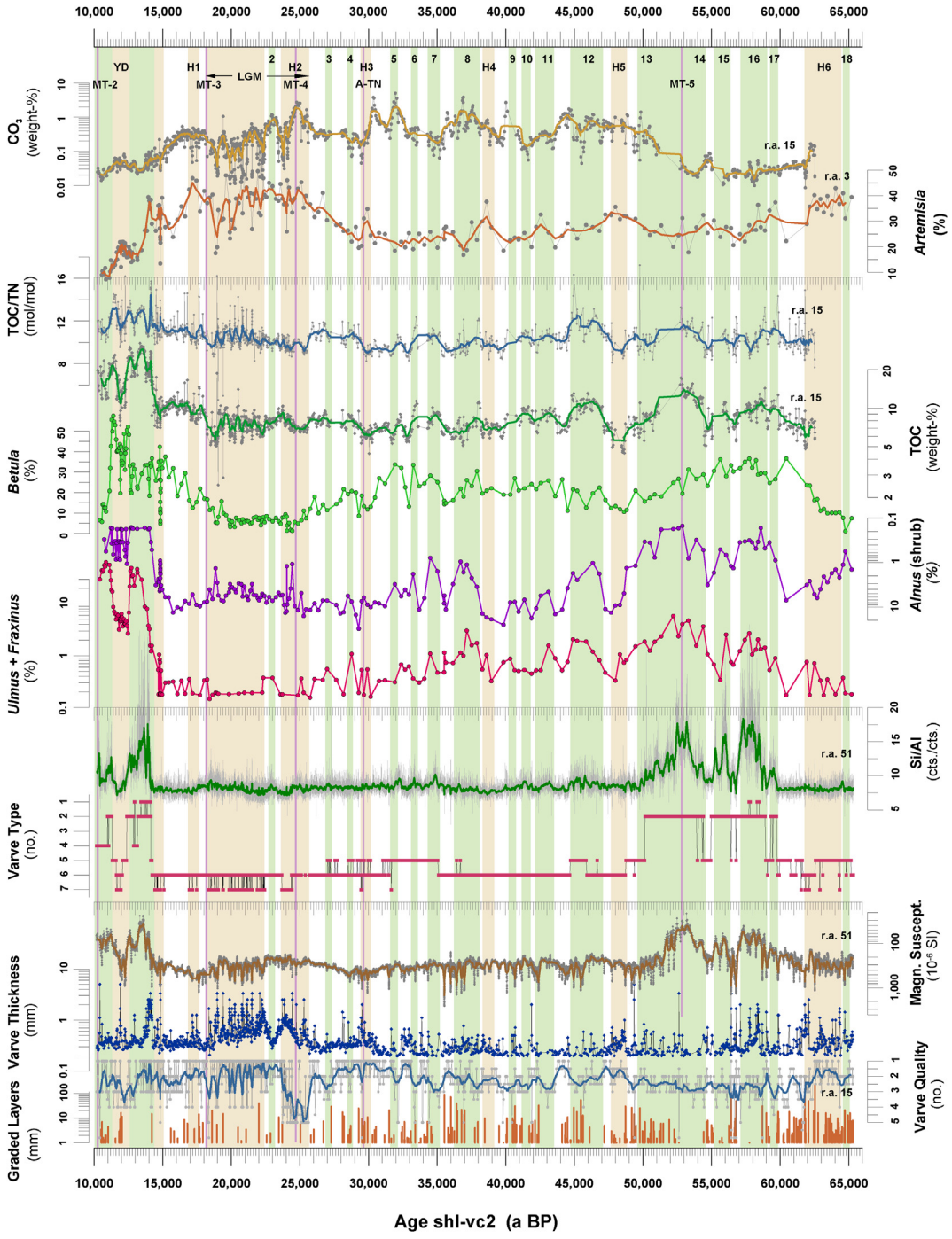

Fig. 6. Lake Sihailongwan sediment data plotted against shl-vc2 age. Vertical green bars – periods with climate amelioration, vertical ochre bars – periods with climate deterioration as deduced from SHL sediment data, vertical violet lines – prominent SHL tephra layers. Numbers beneath topmost age scale indicate equivalents of Greenland Dansgaard-Oeschger cycles; YD – Younger Dryas equivalent; H1–H6 – Heinrich event equivalents; LGM – Last Glacial Maximum at SHL; MT – marker tephra; A-TN – Aira-TN tephra; r.a. = running average, applied for the thicker, colored lines. Note: values of magnetic susceptibility and Alnus percentages are plotted on an inverse scale. Ulmus + Fraxinus and Alnus (shrub) pollen percentage data: zero values not shown due to the logarithmic scale. Varve type numbers as defined in Table 2. Varve quality numbers as defined in text (Section 4.1.1. "Varves"), with lower numbers representing better preservation. Graded Layers: shown are Type-I graded event layers with reworked terrestrial plant litter as defined in text (Section 4.1.2. "Graded event layers"). Only layers with layer thickness ≥1 mm are shown. (For interpretation of the references to color in this figure legend, the reader is referred to the Web version of this article.)

4.3. Sediments and palaeoenvironmental conditions

The TOC concentration of lake sediments depends on the autochthonous biogenic production, organic matter preservation, and the influx of allochthonous minerogenic matter. The balance of autochthonous productivity and terrestrial input of higher plant litter is reflected by the ratio of total organic carbon to total nitrogen (TOC/TN ratio). TOC/TN ratios of non-vascular aquatic plants (i.e. algae) typically range between 4 and 10, while these ratios are above 20 for higher plants (Meyers and Ishiwatari, 1993). Increasing TOC/TN ratios thus reflect increased terrestrial input and/or decreased autochthonous productivity, with a tendency to elevated

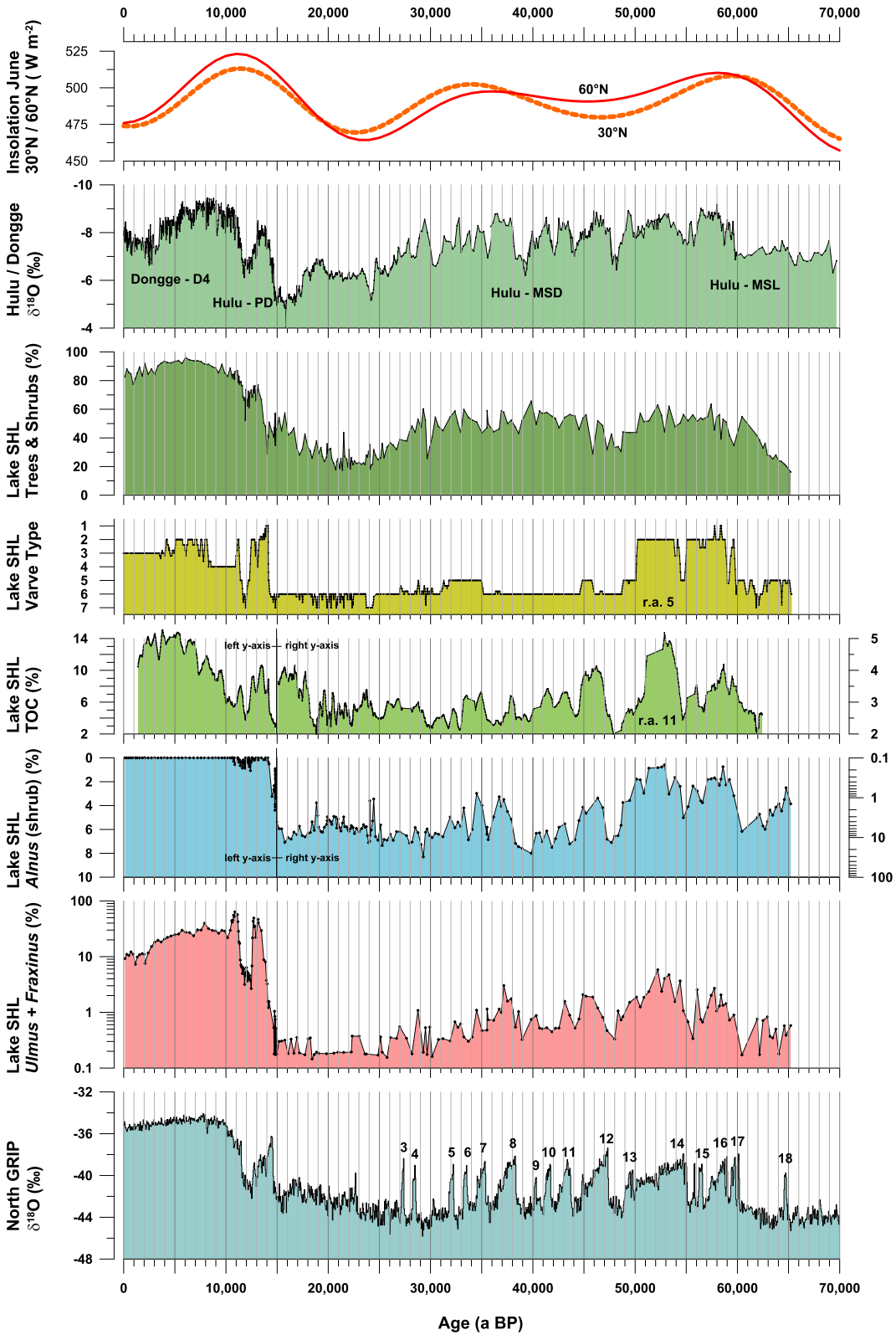

Fig. 7. Comparison of selected Lake Sihailongwan data, Greenland ice core oxygen isotope data (from: Members N. G. I. C. P., 2004), Chinese speleothem oxygen isotope data (from: Dykoski et al., 2005 (Dongge-D4); Wang et al., 2001 (Hulu-Cave PD, MSD, MSL)), and Northern Hemisphere insolation data (after Berger and Loutre, 1991) for the last 70 ka. Note: *Alnus* percentages are plotted on an inverse scale. TOC (and *Alnus*) data are plotted against two different percentage scales (y-axes) to highlight differentiation at lower (higher) values during the Last Glacial.

values with increasing time caused by the preferential decomposition of nitrogen-containing compounds during diagenesis. Total organic carbon content of the SHL sediments varies between 3 and 5%, with TOC/TN ratios typically between 8 and 12, pointing to a mixture of terrestrial and aquatic biogenic components. Exceptions are graded event layers of Type I with enrichment of terrestrial plant remains and TOC/TN-ratios rising up to >20 (Figs. 4c and 6).

Carbonate contents of the sediments are low but variable, at values between 0.1 and 2% CO_3^{2-} for most of the Last Glacial and nearly zero values occur during the warmer interstadials 13 to 17 and the LGM. Some samples have been investigated by SEM-EDX mapping (not shown) and revealed siderite ($FeCO_3$) as the only carbonate phase which agrees well with thin section observations. Assuming similar hydro-chemical characteristics of the modern SHL compared to Last Glacial lake and in general lower but still existent lake productivity, the formation of authigenic siderite under anoxic conditions is favoured by the low SO_4^{2-} concentration of SHL lake water (Schettler et al., 2006a) which relates to a strong limitation in H_2S release rates. However, formation of authigenic Fe-minerals requires a pool of reactive iron originating from inflow of external weathering solutions, input by aeolian influx or in-situ release by chemical mineral alteration.

If primary influx of inorganic carbon is diminished and soil carbonates are leached during subsequent wetter periods, carbonate content decreases towards zero values. Hence carbonate content of Last Glacial SHL sediments can reflect dry periods in dust source areas as well as increased precipitation at SHL. The restriction of carbonate occurrence in SHL sediments to the Last Glacial points to remote dust as a possible carbonate source and low autochthonous biogenic production to preserve the carbonates (Dean, 1999).

The Si/Al ratio of lake sediments is an indicator of limnic autochthonous productivity of organisms with silicon-based skeletons and shells (Peinerud, 2000; Jenny et al., 2013; Wolff et al., 2014), which in SHL are mostly diatoms (varve types 1 to 5) with smaller contributions of chrysophyceae cysts and scales (varve type 6).

Typical varves of the Last Glacial exhibit a distinct clastic spring melt layer composed of remote aeolian material trapped on lake ice and snow-melt surface runoff from the catchment, a mixed summer layer with varying, but mostly low amounts of lake biota, and a fine-grained winter layer composed of clay minerals and some additions of decomposed organic matter and xenomorphic siderite (varve types 5 and 6, Fig. 3 (5–6) and Fig. 4a). The most pronounced exception occurs between 60 and 50 ka BP with an evidently much higher productivity of the lake as in particular expressed in varve types (varve types 2 and even 1 for a short period) and much increased Si/Al ratios. Another exceptional period between 24 and 18.5 ka BP exhibits purely minerogenic varves of type 7 (Table 1, Figs. 3, 5 and 6).

For large parts of the Last Glacial the pollen sum of trees and shrubs is between 40% and 50% (Fig. 7), indicating a landscape with patchy forest comparable to the modern “woodland steppe ecotone” of south-eastern Inner Mongolia (Liu et al., 1999; Stebich et al., 2009).

Some of the SHL proxy data from the Last Glacial like TOC content and pollen percentages of selected taxa (e.g. *Fraxinus*, *Alnus*) exhibit pronounced millennial-scale changes, very similar in timing and amplitude to the well-known Dansgaard-Oeschger (D-O) cycles from Greenland ice cores. Based on these observations we divide the description of results into stadials and interstadials parallel to millennial-scale $\delta^{18}O$ variations – interpreted as temperature changes - recorded in Greenland ice cores for the Last Glacial and the Late-glacial period (Dansgaard et al., 1993; Björck et al., 1998; Svensson et al., 2008) (Fig. 6).

4.3.1. Last glacial interstadials

Annual laminations of interstadial periods exhibit a large variety of types between nearly pure clastic varves and varves dominated by thick diatom laminae. The magnetic susceptibility record shows two periods with extremely low values in the middle and lower (Last Glacial) part of the SHL profile (Figs. 2 and 6), with only the younger period being subject of this paper. Low values of magnetic susceptibility result from combined effects of lower influx of minerogenic matter, dilution by higher amounts of organic matter, and enhanced dissolution of magnetic carriers due to longer lasting reducing conditions in the deep water.

Sediment thin sections contain pronounced seasonal diatom layers as the main characteristic of these periods. As the older of these periods at about 35.6–34.2 m profile depth is out of range of the present chronology, we only discuss the two distinct, but shortly following each other and succeeding phases between 59 and 51 ka BP. Varves here composed of a spring melt layer, immediately followed by a thick diatom layer which is usually dominated by *Stephanodiscus parvus/minutulus*, and a mixed layer. The latter is composed of terrestrial organic detritus, a variety of diatom species including redistributed benthic ones, and allochthonous minerogenic matter. Varves at the onset of the productive interstadial strongly resemble those at the beginning of the Late-glacial period, with enrichments of vivianite and up to several mm-thick seasonal (spring) diatom layers (varve type 1). The very large abundance of small-sized *Stephanodiscus* indicates high phosphorus supply and would indicate deep mixing of the water column in spring, as this limnological process can re-cycle nutrients including those released from the sediment under anoxic conditions. Large blooms of *Stephanodiscus* most likely occur under the following scenario: late, rapid ice-out with deep but short mixing of the water column and a rapid onset of thermal stratification driven by rapid warming in spring (Koutsodendris et al., 2013; Kienel et al., 2017). At the end of the productive period between 52 and 51 ka BP diatom blooms are more often composed of *Cyclotella*, *Aulacoseira subarctica*, and sporadically also *Fragilaria gracilis*. Assemblages dominated by small-sized *Cyclotella* and *Discostella* would indicate lower supply of phosphorus and less intense, shallower spring mixing compared with that dominated by *Stephanodiscus*. *Aulacoseira subarctica*, that is most abundant at ~57 ka BP, benefits from a scenario in which ice-cover is short, ice-out early and spring circulation is long lasting. This is because this diatom species is better able to sustain large population under turbulent, low-light conditions than the other planktonic diatoms present in the sequence. However, this advantage may be lost if further warming causes an early onset of summer stratification (Horn et al., 2011).

Some components of the local vegetation obviously react on millennial-scale climatic changes as evidenced by variations of thermophilous species (e.g. *Ulmus* and *Fraxinus*) and the pioneer shrub *Alnus*. Thermophilous elements (*Alnus*) show most pronounced increases (decreases) in interstadials. Prevailing varve types 1 and 2 as well as high Si/Al ratios document a highly productive lake between 60 and 50 ka BP (Fig. 6).

Graded event layers (Figs. 4 and 6) are largely absent during these most pronounced interstadials (as during the Late-glacial warming and the Holocene), which is, together with a massive increase of lake productivity (as seen in varve types and Si/Al ratios), a strong hint for non-permafrost conditions. Particularly varves of type 1 with extremely high accumulation rates of biogenic silica strongly support this, as they are explained by increased influx of freshly released nutrients previously bound in the SHL catchment under dry and cold climatic conditions, most probably in deeply frozen soils. Alternatively, changing precipitation/evaporation ratios from colder into warmer periods could have forced increased groundwater inflow and mobilization of nutrients from

dry deep soils. However, such a scenario would not explain the pronounced difference in lake productivity between D-O 17-13 (very high) and e.g. 12-8 (low) (Fig. 6). The regional pollen signal does not show such a pronounced difference between D-O 17-13 and D-O 12-8 which calls for a local threshold in particular hindering groundwater inflow into the lake.

Some minor, but distinct fluctuations of thermophilous taxa and *Alnus* between 47.5 and 31.5 ka BP are accompanied only in some cases by minor changes in the productivity of the lake as defined mainly by (more diatom-rich) varve types (Fig. 6). Varves of these less pronounced interstadials alternate between type 5 and 6, having only limited amounts of lake biota and differ mainly in predominance of diatoms (varve type 5) or chrysophyte stomatocysts (varve type 6). TOC exhibits increased values for the interstadial between 47.3 and 44.5 ka BP (equivalent to D-O 12), but there is no TOC increase for the pollen-defined interstadial between 38.3 and 36.2 ka BP (equivalent to D-O 8).

4.3.2. Last glacial stadials

Varves from colder and/or dryer phases of the Last Glacial (stadials) are mostly of very uniform character and are typically composed of a silt-sized, clastic-minerogenic base (spring melt-layer), a mixed layer dominated by minerogenic supply as well, and a winter clay layer with varying amounts of siderite and decomposed organic matter. They do not differ from varves of interstadials with slightly enhanced percentages of thermophilous plant taxa. Limnic organogenic remains are diatoms, but frequently also stomatocysts and scales of chrysophytes predominate (varve types 5 and 6).

During all stadials and interstadials with low lacustrine productivity (between 15 ka BP and 50 ka BP) varying amounts of carbonates (0.1–1% CO_3) are present as siderite, mostly in winter layers. However, in detail there are no relations with other parameters like TOC, pollen percentages, or magnetic susceptibility, which points to complex conditions required for carbonate formation and preservation in SHL as discussed above. The frequent occurrence of Type-I graded event layers with reworked soil material during all stadial periods (Fig. 6) suggests prevailing unstable top-soil conditions - probably due to permafrost in the catchment area.

Before 61.5 and after 24 ka BP (and for a short period of only three decades at about 29.6 ka BP, and some decades between 14.9 and 14.5 ka BP) varve thicknesses are substantially enhanced (Fig. 6). Varves during these periods are of clastic-minerogenic origin (type 7). They frequently exhibit clear normal gradation ending with a pronounced winter clay layer. Remains of limnic organisms are restricted to chrysophyte stomatocysts and -scales, which are known to be enriched within seasonal layers and thus can serve as additional indicator of varved lake sediments (Zeeb and Smol, 2001). Occasional occurrences of sponge spicules point to clear-water conditions in the lake (Frost, 2001). Except for the clastic varves mentioned above, the water depth of SHL should have been more than 26 m for most of the Last Glacial if we take into consideration observations from the recent transect with gravity cores showing no varves above 26 m water depth, presuming largely comparable mixing conditions within the small maar lake.

In concordance with limnological indicators, pollen data document cold and dry climatic conditions before 61.5 and after 25.6 ka BP until the Late-glacial period as evidenced e.g. by increased *Artemisia* and decreased *Betula* pollen percentages as well as decreased pollen sum of trees and shrubs (Figs. 6 and 7).

4.3.3. The Last Glacial Maximum and the transition into the late-glacial period

Between 25.6 and 18.2 ka BP sedimentation rates are enhanced due to higher minerogenic influx (expressed in higher varve thickness and magnetic susceptibility values, varves of types 6 and 7). The pollen spectrum with lowest (basically zero) values of thermophilous taxa such as *Ulmus* and *Fraxinus*, increased amounts of *Artemisia*, and lowest percentages of *Betula* pollen as well as total tree and shrub pollen (Figs. 6 and 7) between 25.6 and 18.2 ka BP point to the coldest climatic conditions during the last 65 ka in N.E. China, representing the LGM. At the beginning of the LGM, between 25.6 and 23.6 ka BP, a section with partly not preserved lamination (Fig. 6 - varve quality index) could be a hint for a lowered lake level due to dryer and/or cooler summer conditions causing less stable stratifications with easier and more frequent lake water mixing leading to destruction of varves by oxygen-demanding bottom dwellers. In the middle of the LGM, between 23.5 and 22.5 ka BP, varves exhibit a regular glacial lamination of type 6 with much thinner varves than below and above, but pollen-as well as TOC-data do not show marked changes compared to the extreme conditions during the previous two millennia. The less frequent occurrence or absence of graded event layers with terrestrial plant remains during the LGM could have been caused by drier climate conditions with less frequent heavy precipitation events.

From about 18.2 ka BP regular and thin varves of the main glacial varve type 6 are dominating the SHL sediments again. Varve thickness, and thus sedimentation rate, is lower than before. The base-line of the magnetic susceptibility goes higher than before, probably reflecting a better preservation of fine-grained magnetic carriers. Palynological data, with increasing *Betula* pollen percentages and slightly increasing percentages of thermophilous trees like *Ulmus*, show a return to conditions like before the LGM. Hence, both sediment and pollen data suggest a climatic amelioration compared to the preceding period.

Between 17.3 and 16.8 ka BP and again shortly before the onset of the Late-glacial period warming, between 14.7 and 14.3 ka BP, frequent changes between finely laminated sediments (varve type 6) and periods dominated by purely clastic-minerogenic sediments (varve type 7, Fig. 3(7) and 4(B)) occur. The latter, lasting typically between 30 and 50 years, points to very unstable climate conditions at a decadal scale, probably related to the wind regime responsible for transport of remote aeolian material to the lake. The 17.5–17 ka BP - interval is additionally characterized by increased *Artemisia* and decreased *Betula* pollen percentages.

Main features of the Late-glacial period and Holocene SHL record have been published already in Schettler et al. (2006a, b, c), Stebich et al. (2009, 2015) and Zhu et al. (2013). Here we only briefly stress some similarities and differences with the Last Glacial changes discussed above. At first glance, the higher (lower) percentages of *Ulmus* and *Fraxinus* (*Alnus* and *Artemisia*) from both, Late-glacial period warming and YD-like climate deterioration, can be compared very well with data from Last Glacial interstadials (stadials).

Shortly after the beginning (ca. 300 years) of the Late-glacial period warming limnic productivity increased as shown by Si/Al-ratios and the occurrence of varve-type 1 with thick seasonal diatom layers (Fig. 6). This feature is very similar to the high-productivity period between 59 and 58 ka BP and points to much enhanced nutrient influx after a long-lasting dry/cold period.

During the YD-like climate deterioration productivity is limited again, and clastic varve types with high magnetic susceptibility reappear, similarly to Last Glacial stadial periods.

5. The monsoon record of Lake Sihailongwan in a regional and global context

The long SHL sediment record with a chronology based on varve counting, calibrated AMS radiocarbon dates of plant macro-fossils

and tephrochronology allows a detailed comparison with regional and global environmental records without tuning. Moreover, the dynamics of environmental change at tie points between different climatic modes can be estimated with great precision due to the nearly continuous seasonal lamination of the whole SHL sediment record.

5.1. The last glacial (65-29.5 ka BP)

Precisely dated monsoon records of the Last Glacial from the East Asian mainland with pronounced millennial-scale variability are almost exclusively from speleothems, i.e. from Hulu Cave (Wang et al., 2001), Dongge Cave (Yuan et al., 2004; Dykoski et al., 2005), and Sanbao Cave (Wang et al., 2008). Other records like loess and lake sediment profiles are hampered by either insufficient dating, proxy uncertainties, and/or discontinuous sedimentation.

Sedimentological, palynological, and geochemical data from the Last Glacial SHL record plotted against depth exhibit variations with large amplitudes (Fig. 2). Applying the shl-v2 chronology, TOC percentages and pollen data of some terrestrial plants show millennial scale patterns well known from palaeoclimate archives of the North Atlantic region (Figs. 6 and 7). Their timing appears to be synchronous with the published Greenland ice core stratigraphy based on the layer-counted GICC05 chronology back to 60.2 ka b2k (before 2000 AD) and the model-based GICC05modelext chronology for the record older than 60.2 b2k (Vinther et al., 2006; Rasmussen et al., 2006, 2014; Andersen et al., 2006; Svensson et al., 2008) (Fig. 7). The match with the Hulu Cave isotope record at the onset of GIS 17 (SHL at 59.8 ka BP using varve types, Hulu cave $\delta^{18}O$ data at 60 ka BP after Wang et al., 2001 and Southon, 2004) is perfect within dating uncertainties of the two sites, which are app. 1000 km off each other in north-south direction. For the later interstadials the SHL chronology supports the “older” of the two presented correlations of GIS 9 through 13 between Hulu Cave and Greenland ice cores (Wang et al., 2001), with the transition between H5 and GIS 12 between 47 and 48 ka BP, supporting the view of Southon (2004).

In particular, but with inverse relation, *Alnus* pollen data mirror D-O cycles 18 to 5 (Figs. 6 and 7). Known environmental requirements of *Alnus* match conditions at SHL during stadial periods of the Last Glacial with more unstable soils and open vegetation, but sufficient soil moisture related to low evapotranspiration. During interstadials, decrease of light-demanding *Alnus* can be explained by both increased pressure of other trees and changing climate, in particular rising temperatures and increased evapotranspiration (Tarasov et al., 2005).

High values of *Artemisia*, a typical dry-tolerant steppic species, and/or predominantly clastic varve types and lowered TOC contents centered at 17.2, 25, 30, 38.7, 48.2 and 61.8–64.7 mirror closely the timing of North Atlantic Heinrich events 1 to 6 (Figs. 6 and 7; H1 to H6, Hemming, 2004 and citations therein). From the East Asian monsoon area cold/dry periods corresponding with Heinrich events have been recorded mainly from different loess-derived parameters like grain size variations (e.g. Porter and An, 1995; Xiao et al., 1995), chemical weathering indices (Guo et al., 1996), or phytolith-based mean annual temperature (MAT) and mean annual precipitation (MAP) reconstructions (Lu et al., 2007), which represent seasonal variations of winter (grain size) as well as summer (weathering indices) or annual (MAT, MAP) monsoon strengths. Speleothem isotope records of MIS 2 and 3 from Hulu Cave (Wang et al., 2001) exhibit excursions towards dryer conditions corresponding with Heinrich events as well. Compared with the Hulu Cave data, SHL *Artemisia* pollen counts show striking similarities in amplitudes of some dry periods. Dry periods corresponding to H3, H4, and H5 are in both records much more expressed than those corresponding to stadials without Heinrich events. Also concordant with speleothems and SHL data are the reconstructions of mean annual temperature and mean annual precipitation based on phytoliths (Lu et al., 2007). They show a clear parallelism between the coldest and driest periods and Heinrich events. These observation from the Chinese mainland are supported by data from the South China Sea, where strong salinity increases have been recorded in particular parallel to H4 and H5 (Bühring et al., 2004). Altogether, there is evidence for a weakening of the East Asian monsoon climate for Heinrich event stadials regardless of their position with respect to precessional insolation forcing. This picture is in contrast to Greenland ice core oxygen isotope variations were negative oxygen isotope excursions are more (GISP2 ice core record) or at least equally expressed (GRIP and North-GRIP ice core records) for the stadials between H3, H4, and H5 compared with those directly associated with Heinrich events (e.g. Seierstad et al., 2014).

During D-O cycles 17 to 13, a pronounced increase of lake productivity calls for substantially enhanced nutrient influx for SHL, which could be maintained only via enhanced groundwater inflow (Schettler et al., 2006a; c) requiring absence of permafrost or at least a substantial deepening of the active layer (van Everdingen, 1998) and sufficient precipitation. The slight, but distinct increase of thermophilous taxa as well as the decrease of cold-adapted *Alnus* in the SHL record evidences elevated temperatures, not only precipitation, during the growing season. Subsequent D-O cycles 12 to 6, although visible in SHL pollen data, lack clear evidence from lake productivity as expressed in varve types and Si/Al ratios (Fig. 6). However, Hulu Cave speleothems, and in particular D-O 8, do not exhibit marked differences in amplitudes of $\delta^{18}O$ data compared to D-O 17 to 13 (Wang et al., 2001). Presuming their interpretation as a proxy for EASM conditions holds true for all interstadials without large variation, the lack of SHL's response to increased precipitation during the later interstadials can be explained most likely by lower temperatures and/or shorter duration of interstadial warming, not allowing for substantial reduction of permafrost and consequently nutrient flux into the lake. Alternatively dry conditions could hinder nutrient influx locally, but the pollen data do not give evidence for this option. Reconstruction of mean annual temperature and mean annual precipitation for the Weinan loess section (Central Loess Plateau) based on phytoliths also reveal D-O 17 to 13 as the wettest and warmest periods during MIS 4 – MIS 3 (Lu et al., 2007). From lacustrine sediments of the Takano Formation in central Japan Tawara et al. (2006) showed D-O cycles 17 to 13 to be much more pronounced – with respect to organic carbon content - than later D-O cycles, very similar to the SHL record. Consequently, terrestrial archives preserve signals of temperature and precipitation change closely related to precessional insolation forcing (Fig. 7). There are no substantial differences in timing and intensity of monsoonal fluctuations reconstructed from terrestrial archives throughout at least eastern China and Japan for this time. Similarly, marine sediments from the Sea of Japan exhibit D-O 14 as the strongest amongst all interstadials of the last 75 ka (Tada et al., 1999; Ikehara and Itaki, 2007). Dark layers in sediments from the Sea of Japan during MIS 3–5 represent periods of high precipitation rates leading to low-salinity surface water and reduced deep water formation, which is controlled largely by summer monsoon precipitation. Sediment cores from the northern South China Sea (Bühring et al., 2004) show a comparable pattern with more depleted $\delta^{18}O$ values during D-O 17-13 than during later D-O cycles 12-6, caused by freshwater influx from the Chinese mainland.

At a global scale, the more intense interstadials between 60 and 50 ka BP fit also to elevated sea levels (Lambeck et al., 2002; Siddall et al., 2003), hence it is not only a monsoonal phenomenon but related primarily to large-scale forcing like insolation-driven global

ice volume.

5.2. The Last Glacial Maximum and the transition into the late-glacial period (25.6–14.5 ka BP)

The transition into the LGM starts already at about 29.5 ka BP with steadily decreasing tree pollen amounts, mainly attributable to *Betula* pollen, and increasing *Artemisia* pollen percentages (Figs. 6 and 7). At the same time an abrupt change from a temperate deciduous forest to a boreal conifer forest occurred in central Japan (e.g. Hayashi et al., 2010). Furthermore, there are indications for the coldest period of the whole Last Glacial and the lowest sea level reconstructed from marine sediment cores around Japan (Machida, 1999 and references therein; Yokoyama et al., 2007), concordant with the global sea-level lowstand that started 30 ka ago (Lambeck and Chappell, 2001). At SHL, almost all thermophilous plants had their minimum values between 25.6 and 18.2 ka BP. Higher clastic influx between 25.6 and 23.8 ka BP at SHL (Fig. 6 – varve thickness and varve type) correlates remarkably well with the double-peak of maximal dust concentration in Greenland ice cores (Ruth et al., 2003). The intra-LGM period between 23.6 and 22.8 ka BP with well-developed varves, decreased varve thickness (due to lower allochthonous minerogenic influx) and a slight increase in thermophilous pollen percentages is not documented by any corresponding climate shift from other regional records so far, perhaps due to insufficient temporal resolution, age control or proxy sensitivity. However, as it correlates with the Greenland Interstadial 2 and a methane concentration increase as recorded in Greenland and Antarctic ice cores (EPICA community members, 2006) it could be a so far unrecognized but widespread temperate spell in the East Asian monsoon climate of the LGM.

Soon after the LGM, between 17.6 and 14.5 ka BP, speleothems from four caves (Hulu cave – Wang et al., 2001; Dongge cave – Yuan et al., 2004; Heshang cave - Hu et al., 2005; Songjia cave – Zhou et al., 2008) across south-eastern and eastern China conformably show a prominent phase with heavier $\delta^{18}O$ values interpreted as a very low-EASM period, the so-called Weak Monsoon Interval (WMI, Cheng et al., 2016). This period parallels the North Atlantic Heinrich Event H1 and the so-called Mystery Interval (Denton et al., 2006; Zhou et al., 2008). The 17.6-14.5 ka BP change has also been referred to as the coldest phase since the LGM (Zhou et al., 2008). SHL data at least do not support a hypothesis of a long-lasting very dry period for NE China. The predominance of thin and well-developed varves (type 3) during this period is a hint for a stable and higher lake level than during most of the LGM. However, a peak in *Artemisia* pollen percentages between 17.65 and 16.85 ka BP and a negative excursion in *Betula* pollen amounts and TOC content correlates well with Heinrich event H1 (Fig. 6), like previous *Artemisia* peaks of MIS 2 and 3 do with older Heinrich events. Later on, for a short period between 14.9 and 14.5 ka BP, the East Asian monsoon system seems to be more unstable again, and varve microfacies and palynological data (Stebich et al., 2009) point to abrupt lake level variations with decades of increased clastic-minerogenic sediment influx.

Slowly increasing TOC- as well as total trees and shrubs percentages since about 18.2 ka BP and decreasing CO_3 values since 16.5 ka BP (Fig. 6) are hints for a slow regional climatic amelioration in concordance with increased northern summer insolation. At orbital time scales, monsoon intensity has been shown to vary with precession (e.g. Kutzbach, 1981; Wang et al., 2001), and the SHL sediment total trees and shrubs percentage data exhibit this relationship as well. From clay content estimations of marine cores from the northern South China Sea, Wang et al. (1999) deduced increased fluvial runoff and concluded that the summer monsoon-intensity preceded the post-glacial sea-level rise by 3000–4000 years in concordance with the summer-insolation increase in the northern hemisphere. However, the impact of these changes on the SHL environment was still minor, and most parameters remained on their Last Glacial levels until the start of the Late-glacial period.

Late-glacial period features of the SHL record mirror the stratigraphic and palaeoclimatic pattern well known from circum – North Atlantic sites (Stebich et al., 2009). The apparent difference in SHL sediment proxy amplitudes between the Late-glacial period and the Last Glacial has been recorded in Chinese speleothems as well (e.g. Ma et al., 2012) and could be assigned to changed climate forcing, in particular to increased summer insolation during the Late-glacial period.

6. Synthesis and conclusions

SHL is a small and deep maar lake with a typical bowl-shaped morphology. In combination with a strongly seasonal climate (extremely cold winters vs. warm, moist summers) this provides best conditions for a long and undisturbed palaeo-monsoon archive. The most prominent and persisting seasonal clock generator for SHL sediments is the ice-out in spring resulting in a clastic-minerogenic snow-melt layer. A combination of varve counting with 50 AMS ^{14}C dates is the backbone for a precise SHL calendar-year chronology (shl-vc2), which allows for regional and hemispheric correlation of palaeoclimate data without tuning.

The SHL record of the Last Glacial documents millennial scale variability of the regional monsoon climate comparable to well-known Greenland ice-core stadials and interstadials. Multiproxy data of SHL biota (TOC, pollen) indicate changes in temperature and precipitation, whereas upstream changes in the isotopic ratios of precipitation alone (as often discussed for the oxygen isotope data of Last Glacial Chinese speleothems, e.g. Johnson and Ingram, 2004) could not cause the observed millennial-scale variability of local limnic proxies and regional vegetation in NE China. The strong response of the limnic system at the transition MIS 4-3 (D-O 17-13), and a massive increase of productivity at the beginning of the Late-glacial period could be related to local nutrient accumulation in the catchment during cold phases with permafrost and their subsequent release in times of climate amelioration. Widespread thawing of permafrost soils at D-O 17-13 compared to only superficially thawed permafrost thereafter provides a plausible explanation of the productivity that is mirrored in proxies predominantly controlled by limnology, as varve types or Si/Al ratios.

Differences between interstadials with and without massive changes in the nutrient budget of the lake could also indicate large-scale differences in the monsoon system, e.g. according to Schiemann et al. (2009) and Chiang et al. (2015) blocking of the Westerlies in southern positions, thus stopping the northward advancement of the front of the summer monsoon. However, currently we cannot quantify to which extend different SHL sediment proxies mirror more local, regional or a mixture of palaeoenvironmental and palaeoclimatic factors. The striking difference between high- and low-nutrient periods of lacustrine sediment proxies (varve type, biogenic silica) was caused by crossing a local threshold within the lake catchment. Whether the monsoon system itself was subject to sudden changes or rather gradual palaeoclimate changes caused the crossing of local thresholds cannot be clarified yet.

Finally, the multiplicity of available sedimentological, geochemical, and biological data has been used to decipher major features of the East Asian Monsoon variability for the last 65 ka:

1. Precessional forcing is evidently important for large-scale variability of the Asian monsoon (Kutzbach, 1981; Wang et al., 2001), and has been recorded in SHL pollen data. However,

there are large differences in response of terrestrial vegetation and lake productivity to the two Northern Hemisphere summer insolation maxima about 60 and 35 ka BP (Fig. 7). The comparison of the June insolation curves for 30°N and 60°N suggests that the intense climate amelioration recorded for SHL between 50 and 60 ka BP could have originated from large-scale internal climate forcing factors, i.e. northern hemispheric ice volume and related sea level as observed already for longer time scales (Liu and Ding, 1993).

2. During the Last Glacial, the SHL TOC content, some thermophilous plants such as *Ulmus* and, on a reversed scale, the pioneer shrub *Alnus* mirror millennial-scale climatic variations known from Greenland ice-cores as D-O-cycles. These stadial/interstadial changes have so far been recognized with great detail in the East Asian mainland only in speleothems, were they have been discussed as variations of summer monsoon intensity or changes in atmospheric circulation patterns. With the SHL record we can show local and regional millennial-scale changes in monsoon intensity, regardless of the origin or transport paths of air masses.
3. Temperature differences amongst interstadials strongly affect sedimentation, most probably mediated by permafrost conditions. During periods with the most intense EASM (equivalent to D-O 13–17), the autochthonous productivity of SHL is comparable with the high productivity phase during the Late-glacial period and much higher than present. Our sediment investigations show that with intensified monsoon during more pronounced interstadials temperatures as well as precipitation are substantially enhanced. Mean annual temperature had to be well above 0 °C and thus comparable to modern values.
4. Last Glacial cold phases, contemporary with North Atlantic Heinrich Events, vary in intensity which points to a close link between the East Asian Monsoon and the North Atlantic climate system.
5. Numerous tephra layers, including a remote volcanic ash layer from Japan, makes the SHL record a key site for regional tephrostratigraphic correlations between the northern Chinese mainland and the Northwest Pacific volcanic arc.

Available chronologies of all long palaeoclimate records, including our SHL record, still lack the precision which would be needed to answer the question whether the driver of millennial-scale oscillations comes from the tropics or from northern latitudes (Clemens, 2006). However, the coincidence in both amplitudes and timing of interstadial events between the SHL record and known D-O cycles from Greenland ice cores suggests a direct, atmospheric connection between the Atlantic and the East Asian Monsoon system during the Last Glacial. Moreover, the occurrence of cold/dry periods at SHL, contemporary with Heinrich events, suggest a major influence of heat-blocking North Atlantic sea ice on atmospheric teleconnections (Seager et al., 2002; Broecker, 2006).

Acknowledgements

The drilling work on Sihailongwan Lake was carried out in the summer of 2001 by a joint team of the GeoResearchCenter Potsdam and the Institute of Geology of the Chinese Academy of Sciences Beijing. Both institutes also financed the drilling work from own resources. For the preparation and execution of the scientific drilling, Prof. J.F.W. Negendank owes special thanks, as well as Prof. Jingtai Han and Prof. Guoqiang Chu. We would like to thank Ingo Heymann, Daniel Acksel and Heiko Howey for their energetic help with the drilling work. Thin-sections were prepared by Dieter Berger and Michael Köhler in the laboratory of the GFZ – German Research Centre for Geosciences, Potsdam.

We would like to thank two anonymous reviewers for the important changes regarding content and style of the paper.

P.R. acknowledges a grant (no. 40872113) from the Natural Science Foundation of China.

The data presented in this manuscript is archived online at PANGAEA® - Data Publisher for Earth & Environmental Science (https://doi.pangaea.de/10.1594/PANGAEA.885907).

References

Andersen, K.K., Svensson, A., Johnsen, S.J., Rasmussen, S.O., Bigler, M., Rothlisberger, R., Ruth, U., Siggaard-Andersen, M.-L., Steffensen, J.P., Dahl-Jensen, D., Vinther, B.M., Clausen, H.B., 2006. The Greenland Ice Core Chronology 2005, 15-42 ka. Part 1: constructing the time scale. Quat. Sci. Rev. 25 (23–24), 3246–3257.

Fang, J.Y., Wang, ZhH., Tang, ZhY. (Eds.), 2009. Atlas of woody plants in China: distribution and climate, first ed. Higher Education Press, Beijing, p. 2020. vol. 4.

Barry, R.G., Chorley, R.J., 1998. Atmosphere, Weather and Climate, seventh ed. Routledge, London, New York, p. 398.

Battarbee, R.W., Jones, V.J., Flower, R.J., Cameron, N.G., Bennion, H., Carvalho, L.R., Juggins, S., 2001. Diatoms. In: Smol, J.P., Birks, H.J.B., Last, W.M. (Eds.), Tracking Environmental Change Using Lake Sediments, Volume 3: Terrestrial, Algal, and Siliceous Indicators. Kluwer Academic Publishers, Dordrecht, The Netherlands, pp. 155–202.

Berger, A., Loutre, M.F., 1991. Insolation values for the climate of the last 10 million years. Quat. Sci. Rev. 10, 297–317.

Berglund, B.E., Ralska-Jasiewiczowa, M., 1986. Pollen analysis and pollen diagrams. In: Berglund, B.E. (Ed.), Handbook of Holocene Palaeoecology and Palaeohydrology. John Wiley and Sons, Chichester, pp. 455–484.

Berner, R.A., 1981. A new geochemical classification of sedimentary environments. J. Sed. Petrol. 51, 359–365.

Björck, S., Walker, M.J.C., Cwynar, L.C., Johnsen, S., Knudsen, K.-L., Lowe, J.J., Wohlfarth, B., Members, Intimate., 1998. An event stratigraphy for the Last Termination in the North Atlantic region based on the Greenland ice-core record: a proposal by the INTIMATE group. J. Quat. Sci. 13 (4), 283–292.

Bony, S., Bellon, G., Klocke, D., Sherwood, S., Fermepin, S., Denvil, S., 2013. Robust direct effect of carbon dioxide on tropical circulation and regional precipitation. Nat. Geosci. 6 (6), 447–451.

Bradbury, J.P., 1988. A climatic-limnologic model of diatom succession for paleolimnological interpretation of varved sediments at Elk Lake, Minnesota. J. Paleolimnol. 1, 115–131.

Broecker, W.S., 2006. Abrupt climate change revisited. Global Planet. Change 54 (3–4), 211–215.

Bühring, C., Sarnthein, M., Erlenkeuser, H., 2004. Toward a high-resolution stable isotope stratigraphy of the last 1.1 m.y.: site 1144, South China Sea. In: Prell, W.L., Wang, P., Blum, P., Rea, D.K., Clemens, S.C. (Eds.), Proceedings of the Ocean Drilling Program, Scientific Results, vol. 184, pp. 1–29.

Cai, W., Santoso, A., Wang, G., Weller, E., Wu, L., Ashok, K., Masumoto, Y., Yamagata, T., 2014. Increased frequency of extreme Indian Ocean Dipole events due to greenhouse warming. Nature 510, 254–258.

Cheng, H., Sinha, A., Wang, X., Cruz, F.W., Edwards, R.L., 2012. The global Paleomonsoon as seen through speleothem records from Asia and the Americas. Clim. Dynam. 39 (5), 1045–1062.

Cheng, H., Edwards, R.L., Sinha, A., Spötl, C., Yi, L., Chen, S., Kelly, M., Kathayat, G., Wang, X., Li, X., Kong, X., Wang, Y., Ning, Y., Zhang, H., 2016. The Asian monsoon over the past 640,000 years and ice age terminations. Nature 534, 640–646.

Chiang, J.C.H., Fung, I.Y., Wu, C.-H., Cai, Y., Edman, J.P., Liu, Y., Day, J.A., Bhattacharya, T., Mondal, Y., Labrousse, C.A., 2015. Role of seasonal transitions and westerly jets in East Asian paleoclimate. Quat. Sci. Rev. 108 (0), 111–129.

Chou, C., 2003. Land-sea heating contrast in an idealized Asian summer monsoon. Clim. Dynam. 21, 11–25.

Chu, G., Liu, J., Schettler, G., Li, J., Sun, Q., Gu, Z., Lu, H., Liu, Q., Liu, T., 2005. Sediment fluxes and varve Formation in sihailongwan, a maar lake from northeastern China. J. Paleolimnol. 34 (3), 311–324.

Chu, G., Sun, Q., Rioual, P., Boltovskoy, A.S., Liu, Q., Sun, P., Han, J., Liu, J., 2008. Dinocyst microlaminations and freshwater "red tides" recorded in Lake Xiaolongwan, northeastern China. J. Paleolimnol. 39 (3), 319–333.

Clemens, S.C., 2006. The Asian Monsoon - extending the historical record by proxy. In: Wang, B. (Ed.), The Asian Monsoon. Springer, Berlin, Heidelberg, New York, pp. 613–630.

Dansgaard, W., Johnsen, S.J., Clausen, H.B., Dahl-Jensen, D., Gundestrup, N.S., Hammer, C.U., Hvidberg, C.S., Steffensen, J.P., Sveinbjörnsdottir, A.E., Jouzel, J., Bond, G., 1993. Evidence for general instability of past climate from a 250-kyr ice-core record. Nature 364, 218–220.

Dean, W.E., 1999. The carbon cycle and biogeochemical dynamics in lake sediments. J. Paleolimnol. 21, 375–393.

Denton, G.H., Broecker, W.S., Alley, R.B., 2006. The mystery interval 17.5 to 14.5 kyrs ago. PAGES Newsletter 14 (2), 14–16.

Domrös, M., Peng, G., 1988. The Climate of China. Springer-Verlag, Berlin, Heidelberg, New York, p. 361.

Duan, F., Wang, Y., Liao, Z., Chen, S., Zhang, W., Shao, Q., 2018. Divergent influences of the Greenland and Antarctica climates on the Asian monsoon during a stadial

to interstadial cycle. J. Asian Earth Sci. 159, 69–73.
Dykoski, C.A., Edwards, R.L., Cheng, H., Yuan, D., Cai, Y., Zhang, M., Lin, Y., Qing, J., An, Z., Revenaugh, J., 2005. A high-resolution, absolute-dated Holocene and deglacial Asian monsoon record from Dongge Cave. China Earth and Planetary Science Letters 233 (1–2), 71–86.
Ellis, C.R., Stefan, H.G., 1989. Oxygen demand in ice covered lakes as it pertains to winter aeration. J. Am. Water Resour. Assoc. 25 (6), 1169–1176.
EPICA community members, 2006. One-to-one coupling of glacial climate variability in Greenland and Antarctica. Nature 444, 195–198.
Fan, Q., Liu, R., Wei, H., Sui, J., Li, N., 1999. The petrology and geochemistry of Jinlongdingzi modern active volcano in Longgang area. Acta Petrol. Sin. 15 (4), 584–589.
Frank, U., 2007. Rock magnetic studies on sediments from erlongwan maar lake, long Gang volcanic field, Jilin province, NE China. Geophys. J. Int. 168 (1), 13–26.
Frost, T.M., 2001. Freshwater sponges. In: Smol, J.P., Birks, H.J.B., Last, W.M. (Eds.), Tracking Environmental Change Using Lake Sediments. Volume 3 - Terrestrial, Algal, and Siliceous Indicators. Kluwer Academic Publishers, Dordrecht, Boston, London, pp. 253–263.
Guo, Z., Liu, T., Guiot, J., Wu, N., Lü, H., Han, J., Liu, J., Gu, Z., 1996. High frequency pulses of East Asian monsoon climate in the last two glaciations: link with the North Atlantic. Clim. Dynam. 12, 701–709.
Hajdas, I., Bonani, G., Zolitschka, B., 2000. Radiocarbon dating of varve chronologies: soppensee and Holzmaar Lakes after ten years. Radiocarbon 42, 349–353.
Haschke, M., 2006. The EAGLE III BKA system, a novel sediment core X-ray fluorescence analyser with very high spatial resolution. In: Rothwell, R.G. (Ed.), New Techniques in Sediment Core Analysis (London Geological).
Hayashi, R., Takahara, H., Hayashida, H.,A., Takemura, K., 2010. Millennial-scale vegetation changes during the last 40,000 yr based on a pollen record from Lake Biwa, Japan. QR (Quat. Res.) (N. Y.) 74 (1), 91–99.
He, Y., Zhao, C., Zheng, Z., Liu, Z., Wang, N., Li, J., Cheddadi, R., 2015. Peatland evolution and associated environmental changes in central China over the past 40,000 years. QR (Quat. Res.) (N. Y.) 84 (2), 255–261.
Hemming, S.R., 2004. Heinrich events: massive late Pleistocene detritus layers of the North Atlantic and their global climate imprint. Rev. Geophys. 42 https://doi.org/10.1029/2003RG000128.
Hofmann, G., Werum, M., Lange-Bertalot, H., 2011. Diatomeen im Süßwasser-Benthos von Mitteleuropa. A.R.G. Gantner Verlag K.G, Ruggell, Liechtenstein.
Horn, H., Paul, L., Horn, W., Petzoldt, T., 2011. Long-term trends in the diatom composition of the spring bloom of a German reservoir: is Aulacoseira subarctica favoured by warm winters? Freshw. Biol. 56, 2483–2499.
Hu, C., Huang, J., Fang, N., Xie, S., Henderson, G.M., Cai, Y., 2005. Adsorbed silica in stalagmite carbonate and its relationship to past rainfall. Geochem. Cosmochim. Acta 69 (9), 2285–2292.
Ikehara, K., Itaki, T., 2007. Millennial-scale fluctuations in seasonal sea-ice and deep-water formation in the Japan Sea during the late Quaternary. Palaeogeogr. Palaeoclimatol. Palaeoecol. 247 (1–2), 131–143.
Jenny, J.-P., Arnaud, F., Dorioz, J.-M., Covex, C.G., Frossard, V., Sabatier, P., Millet, L., Reyss, J.-L., Tachikawa, K., Bard, E., Pignol, C., Soufi, F., Romeyer, O., Perga, M.-E., 2013. A spatiotemporal investigation of varved sediments highlights the dynamics of hypolimnetic hypoxia in a large hard-water lake over the last 150 years. Limnol. Oceanogr. 58 (4), 1395–1408.
Jiang, W., Guo, Z., Sun, X., Wu, H., Chu, G., Yuan, B., Hatte, C., Guiot, J., 2006. Reconstruction of climate and vegetation changes of lake bayanchagan (Inner Mongolia): Holocene variability of the East asian monsoon. QR (Quat. Res.) (N. Y.) 65 (3), 411–420.
Johnson, K.R., Ingram, B.L., 2004. Spatial and temporal variability in the stable isotope systematics of modern precipitation in China: implications for paleoclimate reconstructions. Earth Planet Sci. Lett. 220 (3–4), 365–377.
Karlsson, J., Ask, J., Jansson, M., 2008. Winter respiration of allochthonous and autochthonous organic carbon in a subarctic clear-water lake. Limnol. Oceanogr. 53 (3), 948–954.
Kienel, U., Kirillin, G., Brademann, B., Plessen, B., Lampe, R., Brauer, A., 2017. Effects of spring warming and mixing duration on diatom deposition in deep Tiefer See, NE Germany. J. Paleolimnol. 57 (1), 37–49.
Koutsodendris, A., Lotter, A.F., Kirilova, E., Verhagen, F.T.M., Brauer, A., Pross, J., 2013. Evolution of a Holsteinian (MIS 11c) palaeolake based on a 12-ka-long diatom record from Dethlingen (northern Germany). Boreas 42, 714–728.
Kutzbach, J.E., 1981. Monsoon climate of the early Holocene: climate experiment with the Earth's orbital parameters for 9000 Years ago. Science 214, 59–61.
Lambeck, K., Chappell, J., 2001. sea level change through the last glacial cycle. Science 292, 679–686.
Lambeck, K., Esat, T.M., Potter, E.-K., 2002. Links between climate and sea levels for the past three million years. Nature 419 (6903), 199–206.
Littmann, T., 1991. Dust storm frequency in Asia: climatic control and variability. Int. J. Climatol. 11, 393–412.
Liu, D., Wang, Y., Cheng, H., Lawrence Edwards, R., Kong, X., Wang, X., Hardt, B., Wu, J., Chen, S., Jiang, X., He, Y., Dong, J., Zhao, K., 2010. Sub-millennial variability of Asian monsoon intensity during the early MIS 3 and its analogue to the ice age terminations. Quat. Sci. Rev. 29, 1107–1115.
Liu, D., Wang, Y., Cheng, Y.,H., Edwards, R.L., Kong, X., Li, T.-Y., 2016. Strong coupling of centennial-scale changes of Asian monsoon and soil processes derived from stalagmite $\delta^{18}O$ and $\delta^{13}C$ records, southern China. QR (Quat. Res.) (N. Y.) 85 (3), 333–346.
Liu, H., Cui, H., Pott, R., Speier, M., 1999. The surface pollen of the woodland-steppe ecotone in southeastern Inner Mongolia. Rev. Palaeobot. Palynol. 105, 237–250.
Liu, J., 1988. The cenozoic volcanic episodes in northeast China. Acta Petrol. Sin. 1, 1–10.
Liu, J., Negendank, J.F.W., Wang, W., Guo, Z., Mingram, J., Chu, G., Chen, R., Luo, X., Liu, T., 2000a. Geological characteristics and distribution of maar lakes in China. Terra Nostra (Bonn) 2000/6, 264–273.
Liu, J., Negendank, J.F.W., Wang, W., Chu, G., Mingram, J., Guo, Z., Luo, X., Chen, R., Liu, D., 2000b. The distribution and geological characteristics of maar lakes in China (in Chinese with English abstract). Quat. Sci. 20 (1), 78–86.
Liu, J., Han, J., Fyfe, W.S., 2001. Cenozoic episodic volcanism and continental rifting in northeast China and possible link to Japan Sea development as revealed from K-Ar geochronology. Tectonophysics 339 (3–4), 385–401.
Liu, J., Chu, G., Han, J., Rioual, P., Jiao, W., Wang, K., 2009. Volcanic eruptions in the Longgang volcanic field, northeastern China, during the past 15,000 years. J. Asian Earth Sci. 34 (5), 645–654.
Liu, T., Ding, Z., 1993. Stepwise coupling of monsoon circulations to global ice volume variations during the late Cenozoic. Global Planet. Change 7 (1–3), 119–130.
Liu, Z., Wen, X., Brady, E.C., Otto-Bliesner, B., Yu, G., Lu, H., Cheng, H., Wang, Y., Zheng, W., Ding, Y., Edwards, R.L., Cheng, J., Liu, W., Yang, H., 2014. Chinese cave records and the East Asia summer monsoon. Quat. Sci. Rev. 83 (0), 115–128.
Lotter, A.F., Eicher, U., Siegenthaler, U., Birks, H.J.B., 1992. Late-glacial climatic oscillations as recorded in Swiss lake sediments. J. Quat. Sci. 7 (3), 187–204.
Lotter, A.F., Lemcke, G., 1999. Methods for preparing and counting biochemical varves. Boreas 28 (2), 243–252.
Lu, H.-Y., Wu, N.-Q., Liu, K.-B., Jiang, H., Liu, T.-S., 2007. Phytoliths as quantitative indicators for the reconstruction of past environmental conditions in China II: palaeoenvironmental reconstruction in the Loess Plateau. Quat. Sci. Rev. 26 (5–6), 759–772.
Ma, Z.-B., Cheng, H., Tan, M., Edwards, R.L., Li, H.-C., You, C.-F., Duan, W.-H., Wang, X., Kelly, M.J., 2012. Timing and structure of the Younger Dryas event in northern China. Quat. Sci. Rev. 41, 83–93.
Machida, H., 1999. The stratigraphy, chronology and distribution of distal marker-tephras in and around Japan. Global Planet. Change 21, 71–94.
Maher, B.A., Thompson, R., 2012. Oxygen isotopes from Chinese caves: records not of monsoon rainfall but of circulation regime. J. Quat. Sci. 27 (6), 615–624.
Members N. G. I. C. P, 2004. High-resolution record of Northern Hemisphere climate extending into the last interglacial period. Nature 431 (7005), 147–151.
Merkt, J., 1971. Zuverlässige Auszählungen von Jahresschichten in Seesedimenten mit Hilfe von Großdünnschliffen. Arch. f. Hydrobiol. 69, 145–154.
Metzeltin, D., Lange-Bertalot, H., Soninkhishig, N., 2009. Diatoms in Mongolia. In: Lange-Bertalot, H. (Ed.), Iconographia Diatomologica, Vol. 20. A.R.G. Gantner Verlag K.G., Ruggell, Liechtenstein.
Meyers, P.A., Ishiwatari, R., 1993. Lacustrine organic geochemistry - an overview of indicators of organic matter sources and diagenesis in lake sediments. Org. Geochem. 20, 867–900.
Mingram, J., Allen, J.R.M., Brüchmann, C., Liu, J., Luo, X., Negendank, J.F.W., Nowaczyk, N., Schettler, G., 2004. Maar- and crater lakes of the Long Gang Volcanic Field (N.E. China) - overview, laminated sediments, and vegetation history of the last 900 years. Quat. Int. 123–125, 135–147.
Mingram, J., Negendank, J.F.W., Brauer, A., Berger, D., Hendrich, A., Köhler, M., Usinger, H., 2007. Long cores from small lakes - recovering up to 100 m - long lake sediment sequences with a high-precision rod-operated piston corer (Usinger-corer). J. Paleolimnol. 37 (4), 517–528.
Mingram, J., Frank, U., You, H., Stebich, M., Liu, J., 2009. A widespread East Asian chronomarker (Aira-TN tephra) found in varved maar lake sediments (Sihailongwan and Erlongwan) of the LongGang Volcanic Field (NE China). In: Haller, M.J., Massaferro, G.I. (Eds.), 3rd. International Maar Conference, Malargüe, Asociación Geológica Argentina, pp. 71–72. http://gfzpublic.gfz-potsdam.de/pubman/item/escidoc:239986.
Miyairi, Y., Yoshida, K., Miyazaki, Y., Matsuzaki, H., Kaneoka, I., 2004. Improved ^{14}C dating of a tephra layer (AT tephra, Japan) using AMS on selected organic fractions. Nucl. Instrum. Methods Phys. Res. Sect. B Beam Interact. Mater. Atoms 223/224, 555–559.
Müller, S., Tarasov, P.E., Andreev, A.A., Tütken, T., Gartz, S., Diekmann, B., 2010. Late Quaternary vegetation and environments in the Verkhoyansk Mountains region (NE Asia) reconstructed from a 50-kyr fossil pollen record from Lake Billyakh. Quat. Sci. Rev. 29 (17–18), 2071–2086.
Nagashima, K., Tada, R., Matsui, H., Irino, T., Tani, A., Toyoda, S., 2007. Orbital- and millennial-scale variations in Asian dust transport path to the Japan Sea. Palaeogeogr. Palaeoclimatol. Palaeoecol. 247 (1–2), 144–161.
Nagashima, K., Tada, R., Tani, A., Sun, Y., Isozaki, Y., Toyoda, S., Hasegawa, H., 2011. Millennial-scale oscillations of the westerly jet path during the last glacial period. J. Asian Earth Sci. 40 (6), 1214–1220.
Nakagawa, T., Gotanda, K., Haraguchi, T., Danhara, T., Yonenobu, H., Brauer, A., Yokoyama, Y., Tada, R., Takemura, K., Staff, R.A., Payne, R., Bronk Ramsey, C., Bryant, C., Brock, F., Schlolaut, G., Marshall, M., Tarasov, P., Lamb, H., 2012. SG06, a fully continuous and varved sediment core from Lake Suigetsu, Japan: stratigraphy and potential for improving the radiocarbon calibration model and understanding of late Quaternary climate changes. Quat. Sci. Rev. 36, 164–176.
Nuhfer, E.B., Anderson, R.Y., Bradbury, J.P., Dean, W.E., 1993. Modern sedimentation in Elk Lake, clearwater county, Minnesota. In: Bradbury, J.P., Dean, W.E. (Eds.), Elk Lake, Minnesota: Evidence for Rapid Climate Change in the North-Central United States, vol. 276, pp. 75–96. Geol.Soc.Am.Spec.Paper.
Nowaczyk, N.R., Melles, M., Minyuk, P., 2007. A revised age model for core PG1351 from Lake El'gygytgyn, Chukotka, based on magnetic susceptibility variations

tuned to northern hemisphere insolation variations. J. Paleolimnol. 37 (1), 65–76.
O'Sullivan, P.E., 1983. Annually-laminated lake sediments and the study of Quaternary environmental changes - a review. Quat. Sci. Rev. 1 (4), 245–313.
Oppenheimer, C., Wacker, L., Xu, J., Galván, J.D., Stoffel, M., Guillet, S., Corona, C., Sigl, M., Di Cosmo, N., Hajdas, I., Pan, B., Breuker, R., Schneider, L., Esper, J., Fei, J., Hammond, J.O.S., Büntgen, U., 2017. Multi-proxy dating the 'Millennium eruption' of changbaishan to late 946 CE. Quat. Sci. Rev. 158, 164–171.
Peinerud, E.K., 2000. Interpretation of Si concentrations in lake sediments: three case studies. Environ. Geol. 40 (1), 64–72.
Porter, S.C., An, Z., 1995. Correlation between climate events in the North Atlantic and China during the last glaciation. Nature 375, 305–308.
Prentice, I.C., Guiot, J., Huntley, B., Jolly, D., Cheddadi, R., 1996. Reconstructing biomes from palaecological data: a general method and its application to European pollen data at 0 and 6 ka. Clim. Dynam. 12, 185–194.
Rasmussen, S.O., Andersen, K.K., Svensson, A.M., Steffensen, J.P., Vinther, B.M., Clausen, H.B., Siggaard-Andersen, M.-L., Johnsen, S.J., Larsen, L.B., Dahl-Jensen, D., Bigler, M., Röthlisberger, R., Fischer, H., Goto-Azuma, K., Hansson, M.E., Ruth, U., 2006. A new Greenland ice core chronology for the last glacial termination. J. Geophys. Res. 11 https://doi.org/10.1029/2005JD006079.
Rasmussen, S.O., Bigler, M., Blockley, S.P., Blunier, T., Buchardt, S.L., Clausen, H.B., Cvijanovic, I., Dahl-Jensen, D., Johnsen, S.J., Fischer, H., Gkinis, V., Guillevic, M., Hoek, W.Z., Lowe, J.J., Pedro, J.B., Popp, T., Seierstad, I.K., Steffensen, J.P., Svensson, A.M., Vallelonga, P., Vinther, B.M., Walker, M.J.C., Wheatley, J.J., Winstrup, M., 2014. A stratigraphic framework for abrupt climatic changes during the Last Glacial period based on three synchronized Greenland ice-core records: refining and extending the INTIMATE event stratigraphy. Quat. Sci. Rev. 106, 14–28.
Reimer, P.J., Baillie, M.G.L., Bard, E., Bayliss, A., Beck, J.W., Bertrand, C.J.H., Blackwell, P.G., Buck, C.E., Buck, G.S., Cutler, K.B., Damon, P.E., Edwards, R.L., Fairbanks, R.G., Friedrich, M., Guilderson, T.P., Hogg, A.G., Hughen, K.A., Kromer, B., McCormac, G., Manning, S., Ramsey Bronk, C., Reimer, R.W., Remmele, S., Southon, J.R., Stuiver, M., Talamo, S., Taylor, F.W., van der Plicht, J., Weyhenmeyer, C.E., 2004. INTCAL04 terrestrial radiocarbon age calibration, 0–26 cal kyr BP. Radiocarbon 46, 1029–1058.
Reimer, P.J., Bard, E., Bayliss, A., Beck, J.W., Blackwell, P.G., Bronk Ramsey, C., Buck, C.E., Cheng, H., Edwards, R.L., Friedrich, M., Grootes, P.M., Guilderson, T.P., Haflidason, H., Hajdas, I., Hatté, C., Heaton, T.J., Hoffmann, D.L., Hogg, A.G., Hughen, K.A., Kaiser, K.F., Kromer, B., Manning, S.W., Niu, M., Reimer, R.W., Richards, D.A., Scott, E.M., Southon, J.R., Staff, R.A., Turney, C.S.M., van der Plicht, J., 2013. IntCal13 and Marine13 radiocarbon age calibration curves 0–50,000 years cal BP. Radiocarbon 55 (4), 1869–1887.
Ren, G., 2000. Decline of the mid- to late Holocene forests in China: climatic change or human impact? J. Quat. Sci. 15 (3), 273–281.
Ren, G., Beug, H.-J., 2002. Mapping Holocene pollen data and vegetation of China. Quat. Sci. Rev. 21 (12–13), 1395–1422.
Renberg, I., 1982. Varved lake sediments - geochronological records of the Holocene. GFF (Geol. Foren. Stockh. Forh.) 104, 275–279.
Ruth, U., Wagenbach, D., Steffensen, J.P., Bigler, M., 2003. Continuous record of microparticle concentration and size distribution in the central Greenland NGRIP ice core during the last glacial period. J. Geophys. Res.: Atmosphere 108 (D3), 4098.
Schettler, G., Romer, R.L., Mingram, J., 2004. Lake Sihailongwan - a natural monitor of dust deposition for NE-China. The Pb, Nd, and Sr isotopic record. Eos Trans. AGU, Suppl. 85 (47). Fall Meet. Suppl., GC51D-1072. http://gfzpublic.gfz-potsdam.de/pubman/faces/viewItemOverviewPage.jsp?itemId=escidoc:231742.
Schettler, G., Liu, Q., Mingram, J., Negendank, J., 2006a. Palaeovariations in the East-Asian monsoon regime geochemically recorded in varved sediments of Lake Sihailongwan (Northeast China, Jilin province). Part 1: hydrological conditions and dust flux. J. Paleolimnol. 35 (2), 239–270.
Schettler, G., Mingram, J., Negendank, J.F.W., Liu, J., 2006b. Palaeovariations in the East-Asian Monsoon regime geochemically recorded in varved sediments of Lake Sihailongwan (Northeast China, Jilin province). Part 2: a 200-year record of atmospheric lead-210 flux variations and its palaeoclimatic implications. J. Paleolimnol. 35, 271–288.
Schettler, G., Mingram, J., Liu, Q., Stebich, M., Dulski, P., 2006c. East-Asian monsoon variability between 15000 and 2000 cal. yr BP recorded in varved sediments of Lake Sihailongwan (northeastern China, Long Gang volcanic field). Holocene 16 (8), 1043–1057.
Schiemann, R., Lüthi, D., Schär, C., 2009. Seasonality and Interannual variability of the westerly jet in the Tibetan plateau region. J. Clim. 22 (11), 2940–2957.
Schmidt, R., Höllerer, H., Wallner, G., 1995. A vacuum sampler for subsampling freeze-dried laminated sediments with the application to in situ frozen varves of Mondsee, Austria. J. Paleolimnol. 14, 93–96.
Seager, R., Battisti, D.S., Yin, J., Gordon, N., Naik, N., Clement, A.C., Cane, M.A., 2002. Is the Gulf Stream responsible for Europe's mild winters? Q. J. R. Meteorol. Soc. 128 (586), 2563–2586.
Seierstad, I.K., Abbott, P.M., Bigler, M., Blunier, T., Bourne, A.J., Brook, E., Buchardt, S.L., Buizert, C., Clausen, H.B., Cook, E., Dahl-Jensen, D., Davies, S.M., Guillevic, M., Johnsen, S.J., Pedersen, D.S., Popp, T.J., Rasmussen, S.O., Severinghaus, J.P., Svensson, A., Vinther, B.M., 2014. Consistently dated records from the Greenland GRIP, GISP2 and NGRIP ice cores for the past 104 ka reveal regional millennial-scale δ18O gradients with possible Heinrich event imprint. Quat. Sci. Rev. 106 (0), 29–46.
Shen, C.-C., Kano, A., Hori, M., Lin, K., Chiu, T.-C., Burr, G.S., 2010. East Asian monsoon evolution and reconciliation of climate records from Japan and Greenland during the last deglaciation. Quat. Sci. Rev. 29, 3327–3335.
Siddall, M., Rohling, E.J., Almogi-Labin, A., Hemleben, Ch, Meischner, D., Schmelzer, I., Smeed, D.A., 2003. Sea-level fluctuations during the last glacial cycle. Nature 423 (6942), 853–858.
Sobek, S., Söderbäck, B., Karlsson, S., Andersson, E., Brunberg, A.K., 2006. A carbon budget of a small humic lake: an example of the importance of lakes for organic matter cycling in boreal catchments. AMBIO A J. Hum. Environ. 35 (8), 469–475.
Southon, J., 2004. A Radiocarbon Perspective on Greenland ice-core Chronologies: can we use ice cores for ^{14}C Calibration? Radiocarbon 46 (3), 1239–1259.
Stebich, M., Mingram, J., Han, J., Liu, J., 2009. Late-Pleistocene spread of (cool-) temperate forests in Northeast China and climate changes synchronous to the North Atlantic region. Global Planet. Change 65, 56–70.
Stebich, M., Rehfeld, Kira, Schlütz, Frank, Tarasov, Pavel E., Liu, Jiaqi, Mingram, J., 2015. Holocene vegetation and climate dynamics of NE China based on the pollen record from Sihailongwan Maar Lake. Quarternary Science Reviews 124, 275–289.
Stuiver, M., Reimer, P.J., Reimer, R.W., 2017. CALIB 7.1 [www program]. http://calib.org. (Accessed 21 July 2017).
Sun, C., You, H., He, H., Zhang, L., Gao, J., Guo, W., Chen, S., Mao, Q., Liu, Q., Chu, G., Liu, J., 2015. New evidence for the presence of Changbaishan Millennium eruption ash in the Longgang volcanic field, Northeast China. Gondwana Res. 28 (1), 52–60.
Sun, L., Shen, B., Gao, Z., Sui, B., Bai, L., Wang, S.-H., An, G., Li, J., 2007. The impacts of moisture transport of East asian monsoon on summer precipitation in northeast China. Adv. Atmos. Sci. 24 (4), 606–618.
Sun, X., Chen, Y., 1991. Palynological records of the last 11,000 years in China. Quat. Sci. Rev. 10, 537–544.
Sun, X.-J., Yuan, S.-M., Liu, J.-L., Tang, L.-Y., 1991. The vegetation history of mixed Korean pine and deciduous forests in Changbai Mt. Area, Jilin province, northeast China during the last 13000 years. Chin. J. Bot. 3 (1), 47–61.
Sun, Y., Clemens, S.C., Morrill, C., Lin, X., Wang, X., An, Z., 2012. Influence of Atlantic meridional overturning circulation on the East Asian winter monsoon. Nat. Geosci. 5 (1), 46–49.
Svensson, A., Andersen, K.K., Bigler, M., Clausen, H.B., Dahl-Jensen, D., Davies, S.M., Johnsen, S.J., Muscheler, R., Parrenin, F., Rasmussen, S.O., Röthlisberger, R., Seierstad, I., Steffensen, J.P., Vinther, B.M., 2008. A 60 000 year Greenland stratigraphic ice core chronology. Clim. Past 4 (1), 47–57.
Tada, R., Irino, T., Koizumi, I., 1999. Land-ocean linkages over orbital and millenial timescales recorded in the late Quaternary sediments of the Japan Sea. Paleoceanography 14 (2), 236–247.
Tarasov, P.E., Peyron, O., Guiot, J., Brewer, S., Volkova, V.S., Bezusko, L.G., Dorofeyuk, N.I., Kvavadze, E.V., Osipova, I.M., Panova, N.K., 1999. Last glacial maximum climate of the former soviet union and Mongolia. Clim. Dynam. 15, 227–240.
Tarasov, P.E., Volkova, V.S., Webb III, T., Guiot, J., Andreev, A.A., Bezusko, L.G., Bezusko, T.V., Bykova, G.V., Dorofeyuk, N.I., Kvavadze, E.V., Osipova, I.M., Panova, N.K., Sevastyanov, D.V., 2000. Last glacial maximum biomes reconstructed from pollen and plant macrofossil data from northern Eurasia. J. Biogeogr. 27, 609–620.
Tarasov, P., Granoszewski, W., Bezrukova, E., Brewer, S., Nita, M., Abzaeva, A., Oberhänsli, H., 2005. Quantitative reconstruction of the last interglacial vegetation and climate based on the pollen record from Lake Baikal, Russia. Clim. Dynam. 25 (6), 625–637.
Tawara, T., Kumon, F., Nagahashi, Y., Kakuta, N., Nozue, Y., 2006. Reconstruction of late Pleistocene climate based on total organic carbon (TOC) contents in TKN-2004 core drilled from Takano Formation, central Japan. J. Geol. Soc. Jpn. 112 (9), 568–579 (in Japanese, with Engl. abstr.).
Tian, J., Brown, T., Hu, F.S., 2005. Comparison of varve and 14C chronologies from steel lake, Minnesota, USA. Holocene 15 (4), 510–517.
Troels-Smith, J., 1955. Karakterisering af lose jordater (Characterization of unconsolidated sediments). Danmarks Geologiske Undersogelse 2 (3), 1–73. Rekke IV.
van Everdingen, R., 1998. (revised 2005). Multi-language glossary of permafrost and related ground-ice terms. Boulder, CO: national snow and ice data center/world data center for glaciology. https://globalcryospherewatch.org/reference/glossary_docs/.
Vandenberghe, J., Renssen, H., van Huissteden, K., Nugteren, G., Konert, M., Lu, H., Dodonov, A., Buylaert, J.-P., 2006. Penetration of Atlantic westerly winds into central and east Asia. Quat. Sci. Rev. 25, 2380–2389.
Vinther, B.M., Clausen, H.B., Johnsen, S.J., Rasmussen, S.O., Andersen, K.K., Buchardt, S.L., Dahl-Jensen, D., Seierstad, I.K., Siggaard-Andersen, M.-L., Steffensen, J.P., Svensson, A., Olsen, J., Heinemeier, J., 2006. A synchronized dating of three Greenland ice cores throughout the Holocene. J. Geophys. Res. 111 https://doi.org/10.1029/2005JD006921.
Wang, B., 2006. The Asian Monsoon. Springer, Berlin Heidelberg NewYork, p. 787.
Wang, L., Sarnthein, M., Erlenkeuser, H., Grimalt, J., Grootes, P., Heilig, S., Ivanova, E., Kienast, M., Pelejero, C., Pflaumann, U., 1999. East Asian monsoon climate during the late Pleistocene: high-resolution sediment records from the south China sea. Mar. Geol. 156, 245–284.
Wang, Y.J., Cheng, H., Edwards, R.L., An, Z.S., Wu, J.Y., Shen, C.-C., Dorale, J.A., 2001. A high-resolution absolute-dated late Pleistocene monsoon record from Hulu cave, China. Science 294, 2345–2348.
Wang, Y., Cheng, H., Edwards, R.L., Kong, X., Shao, X., Chen, S., Wu, J., Jiang, X., Wang, X., An, Z., 2008. Millennial- and orbital-scale changes in the East Asian

monsoon over the past 224,000 years. Nature 451, 1090–1093.
Werner, F., 1966. Herstellung von ungestörten Dünnschliffen aus wassergesättigten, pelitischen Lockersedimenten mittels Gefriertrocknung. Meyniana 16, 107–112.
Wetzel, R.G., 2001. Limnology. Academic Press, San Diego, London, p. 1006.
Wolff, C., Kristen-Jenny, I., Schettler, G., Plessen, B., Meyer, H., Dulski, P., Naumann, R., Brauer, A., Verschuren, D., Haug, G.H., 2014. Modern seasonality in Lake Challa (Kenya/Tanzania) and its sedimentary documentation in recent lake sediments. Limnol. Oceanogr. 59 (5), 1621–1636.
Wright, R.F., 1976. The impact of forest fire on the nutrient influxes to small lakes in Northeastern Minnesota. Ecology 57 (4), 649–663.
Xiao, J., An, Z., Kumai, H., Yoshikawa, S., 1995. Grain size of quartz as an indicator of winter monsoon strength on the Loess Plateau of Central China during the last 130,000 yr. QR (Quat. Res.) (N. Y.) 43, 22–29.
Yang, X., Lin, E., Ma, S., Ju, H., Guo, L., Xiong, W., Li, Y., Xu, Y., 2007. Adaptation of agriculture to warming in Northeast China. Climatic Change 84 (1), 45–58.
You, H., Liu, J., Liu, Q., Chu, G., Rioual, P., Han, J., 2008. Study of the varve record from Erlongwan maar lake, NE China, over the last 13 ka BP. Chin. Sci. Bull. 53 (2), 262–266.
Yancheva, G., Nowaczyk, N.R., Mingram, J., Dulski, P., Schettler, G., Negendank, J.F.W., Liu, J., Sigman, D.M., Peterson, L.C., Haug, G., 2007. Influence of the intertropical convergence zone on the East Asian monsoon. Nature 445 (7123), 74–77.
Yokoyama, Y., Kido, Y., Tada, R., Minami, I., Finkel, R.C., Matsuzaki, H., 2007. Japan Sea oxygen isotope stratigraphy and global sea-level changes for the last 50,000 years recorded in sediment cores from the Oki Ridge. Palaeogeogr. Palaeoclimatol. Palaeoecol. 247 (1–2), 5–17.
Yuan, D., Cheng, H., Edwards, R.L., Dykoski, C.A., Kelly, M.J., Zhang, M., Qing, J., Lin, Y., Wang, Y., Wu, J., Dorale, J.A., An, Z., Cai, Y., 2004. Timing, duration, and transitions of the last interglacial asian monsoon. Science 304 (5670), 575–578.
Zeeb, B.A., Smol, J.P., 2001. Chrysophyte scales and cysts. In: Smol, J.P., Birks, H.J.B., Last, W.M. (Eds.), Tracking Environmental Change Using Lake Sediments. Volume 3 - Terrestrial, Algal, and Siliceous Indicators. Kluwer Academic Publishers, Dordrecht, Boston, London, pp. 203–223.
Zhu, J., Mingram, J., Brauer, A., 2013. Early Holocene aeolian dust accumulation in northeast China recorded in varved sediments from Lake Sihailongwan. Quat. Int. 290–291, 299–312.
Zhou, H., Zhao, J., Feng, Y., Gagan, M.K., Zhou, G., Yan, J., 2008. Distinct climate change synchronous with Heinrich event one, recorded by stable oxygen and carbon isotopic compositions in stalagmites from China. QR (Quat. Res.) (N. Y.) 69 (2), 306–315.
Zolitschka, B., Francus, P., Ojala, A.E.K., Schimmelmann, A., 2015. Varves in lake sediments – a review. Quat. Sci. Rev. 117, 1–41.